Datasheet

Rotational Scanning HSI ATH3100

Features

- Rotating scanning imaging with adjustable scanning angle range;
- High-sensitivity hyperspectral imager;
- High-stability, high-blue synthetic lighting source with adjustable power and spectrum;
- High-performance image sensor with excellent cost-effectiveness;
- Full-target high imaging quality optical design with a spot diameter less than 0.5 pixels;
- The objective lens interface is a standard C-Mount, allowing for lens replacement according to user requirements.
- Wavelength range: 400-1000nm, 900-1700nm, or 400-1700nm;
- High spectral resolution: 1.3 nm @ visible light, 3.5 nm @ shortwave infrared;
- Outstanding imaging performance

Application

- Universities and research institutes;
- Biomedical applications;
- Agricultural applications: pest and disease monitoring, nutrient monitoring, disaster assessment, crop yield estimation, etc.;
- Forestry applications: species identification, biomass estimation, nutrient element monitoring, forest health, etc.;
- Water environment applications: inversion of water quality parameters, analysis of spatial distribution and migration characteristics of water pollution;
- Soil monitoring: soil moisture monitoring, soil fertility monitoring;
- Geological applications: mineral mapping, mineral composition detection, mineralization prediction.

Description

Introducing the ATH3100, a compact and lightweight rotational scanning hyperspectral imaging system. This miniature imager boasts high spatial and spectral resolution, complemented by a wide imaging range. It features a high-stability synthetic lighting source with adjustable power and spectral types, ensuring versatile applications in various industries.

The ATH3100 comprises a hyperspectral imager utilizing advanced transmission grating technology for superior aberration correction. Paired with a fully automatic electric rotating stage and four fixed lighting sources, it offers precise imaging capabilities.

Ideal for long-term, large-area scanning, the ATH3100 supports tripod or pole mounting and includes features like automatic calibration and weather monitoring sensors. It meets the demands of environmental monitoring, agriculture, and remote sensing applications, reflecting current trends in hyperspectral imaging technology.

Explore the ATH3100 and revolutionize your imaging capabilities with our cutting-edge rotational scanning hyperspectral imaging systems.

Model	Feature description
ATH3100	Basic model, 370~1000 nm
ATH3100W	Wide field-of-view model, 370~1000 nm
ATH3100-17	Near-infrared hyperspectral, 900~1700 nm
ATH3100-25	Shortwave infrared hyperspectral, 1200~2500 nm
ATH3100-4-17	Wide spectral range, 370~1700 nm

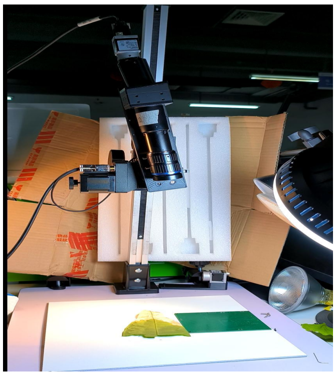

1503 Bld. A04, 3rd Software Park, Jimei, Xiamen, 361005, China
Tel: +86-592-6102588

1. Parameter

Serial Number	Indicator	ATH3100	ATH3100W	ATH3100-17	ATH3100-25
1	Spectral Range	370~1000nm	370~1000nm	900~1700nm	1200~2500nm
2	Best Spectral Resolution	1.3 nm	1.3 nm	3.5nm	7.2nm
3	Sampling Interval	0.37nm	0.37nm	1.56nm	2.54nm
4	F-Number	F/2.6	F/2.6	F/2.6	F/2.6
5	Detector	CMOS	CMOS	InGaAs CCD	Cooling Type InGaAs CCD
6	Detector Interface	USB3.0	USB3.0	USB3.0	USB3.0
7	Detector Power Supply	USB Power Supply, 3.4W	USB Power Supply, 3.6W	12V,14.5W	12V,30W
8	Detector Target Area Size	11.26mm x 5.98mm	11.26mm x 11.26mm	NA	6.4X5.12
9	Detector Raw Resolution	2048 ×1088	2048×2048	640X512	320X256
10	Detector Raw Pixel Size	5.5 μm x5.5 μm	5.5 μm x5.5 μm	15μmx15 μm	20 μm x20 μm
11	Pixel Bit Depth	12 bits	12 bits	14 bits	14 bits
12	Slit Width	25 μm, Other widths available upon customization	25 μm, Other widths available upon customization	30 μm, Other widths available upon customization	
13	Recommended Pixel Merging Method	4x4 or 2x4	4x4 or 2x4	1X2 or None	1X2 or None
14	Spatial Dimension Band Count	512 or 1024	512 or 1024	640	640
15	Spectral Band Count	300 or 600	512 or 1024	512	512
16	Field of View (FOV)	15.2°@f=35mm	15.2°@f=35mm	NA	NA
17	Instantaneous Field of View (IFOV)	0.7mrad @f=35mm	0.7mrad@f=35mm	NA	NA
18	Maximum Frame Rate	340 fps	140 fps	270 fps	270 fps
19	Dimensions	306 mm x300 mm x 162mm	306 mm x300 mm x 162mm	306 mm x300 mm x 162mm	306 mm x 300 mm x 162mm
20	Weight	Less than 8.5 Kg	Less than 85 Ka	Less than 8.8 Kg	Less than 10.5 Kg

1503 Bld. A04, 3rd Software Park, Jimei, Xiamen, 361005, China
Tel: +86-592-6102588

21	Operating Temperature	-10-50℃	-10-50℃	-10-50℃	-10-50℃
22	Storage Temperature	-30-70℃	-30-70℃	-30-70℃	-30-70℃
26	Scanning Method	Rotary push-broom imaging			
27	Data Acquisition Software	Exposure time can be flexibly set, with real-time hyperspectral images and spectral curves dynamically displayed.			
28	Data Analysis Software	No third-party software required; one-click access to clustering analysis, single-band images, false color and true color images, over 20 vegetation indices (customizable), image 3D cropping, and target spectral identification. All functions support unattended batch processing.			
29	Software Display	Dynamic real-time display of hyperspectral images with scientific brightness and focus adjustment to avoid human visual focus errors.			
30	Hyperspectral Camera Communication Method	USB3.0			
31	llumination Light Source	High-stability constant power high-blue synthetic surface light source. Power and spectral type are adjustable (strongly recommended to pair with Optosky ATP9100 for spectral type monitoring).			
32	Number of light sources	2-4 units			
33	Service life (optional)	≥10000h			

1503 Bld. A04, 3rd Software Park, Jimei, Xiamen, 361005, China
Tel: +86-592-6102588

2. ATH3100 Physical Image

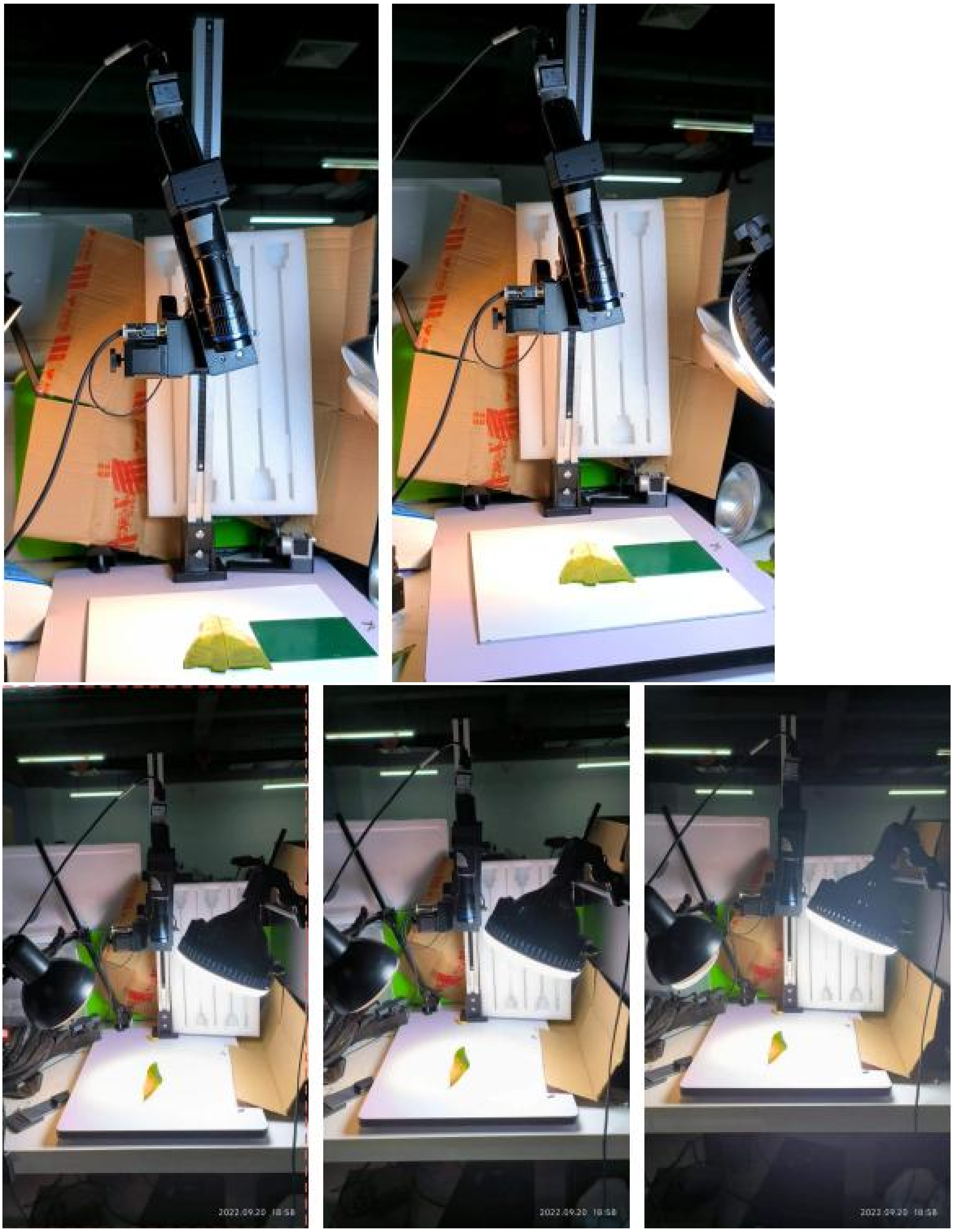

Figure 1: Front view of ATH3100 (The cable at the top is the data line for the hyperspectral imager, while the cable in the middle is the control signal line for the rotating stage.)

1503 Bld. A04, 3rd Software Park, Jimei, Xiamen, 361005, China
Tel: +86-592-6102588

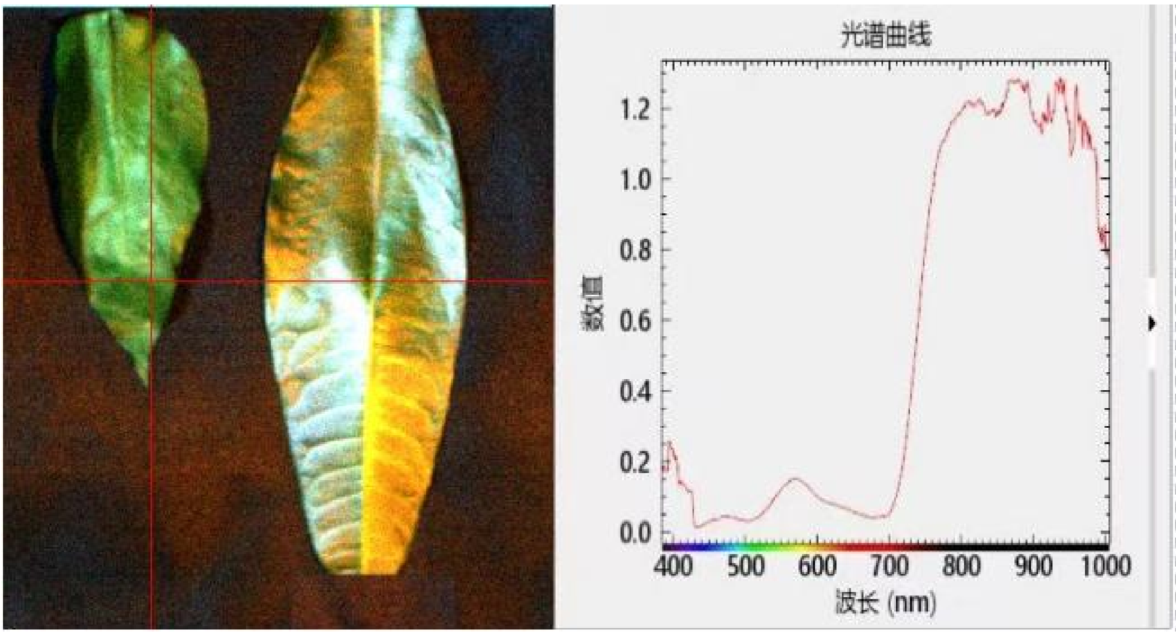

Figure 2: Imaging Effect of ATH3100

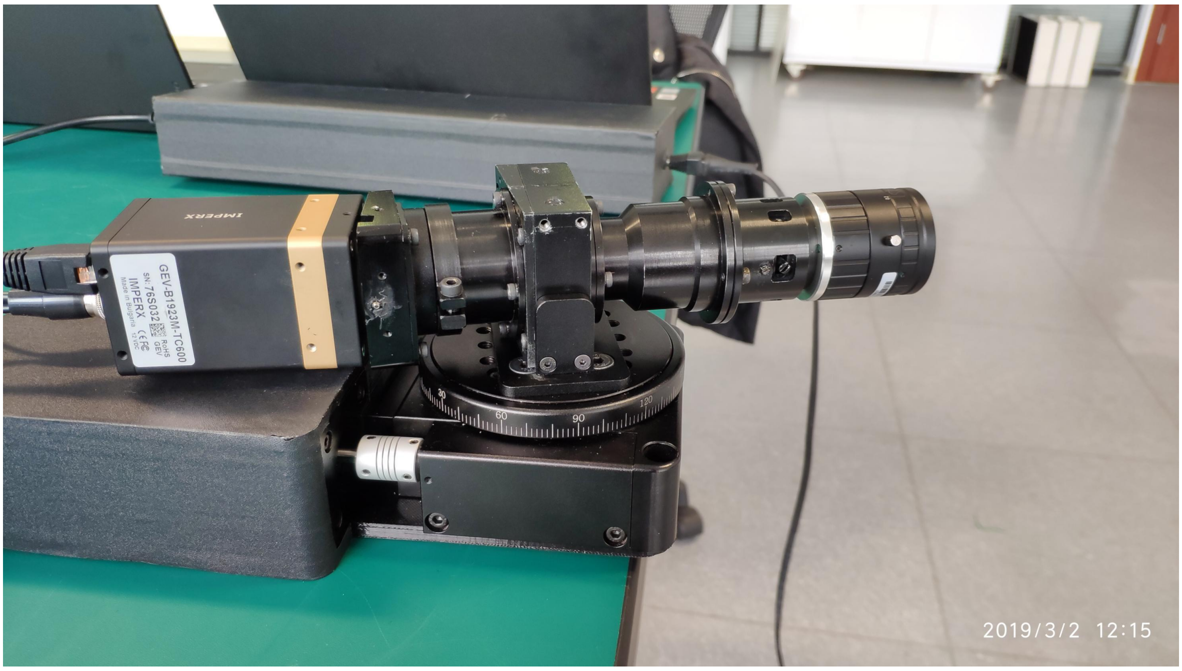

Figure 3: The previous generation of rotational scanning imaging spectrometer produced by Optosky

1503 Bld. A04, 3rd Software Park, Jimei, Xiamen, 361005, China
Tel: +86-592-6102588

3. Application Scenarios

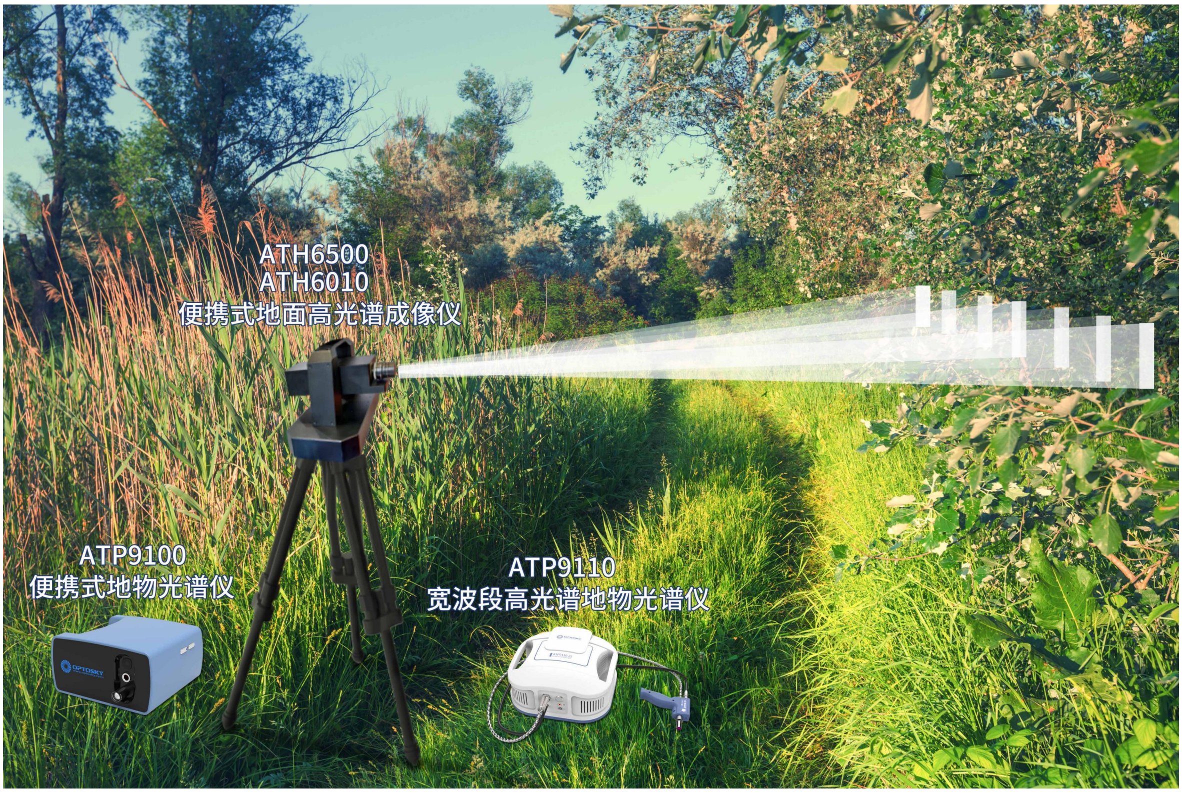

Figure 5: The combined use of hyperspectral imager and ground-based spectrometer

Figure 6: ATH3010OL Field-Based Continuous Hyperspectral Observation System

4.Examples

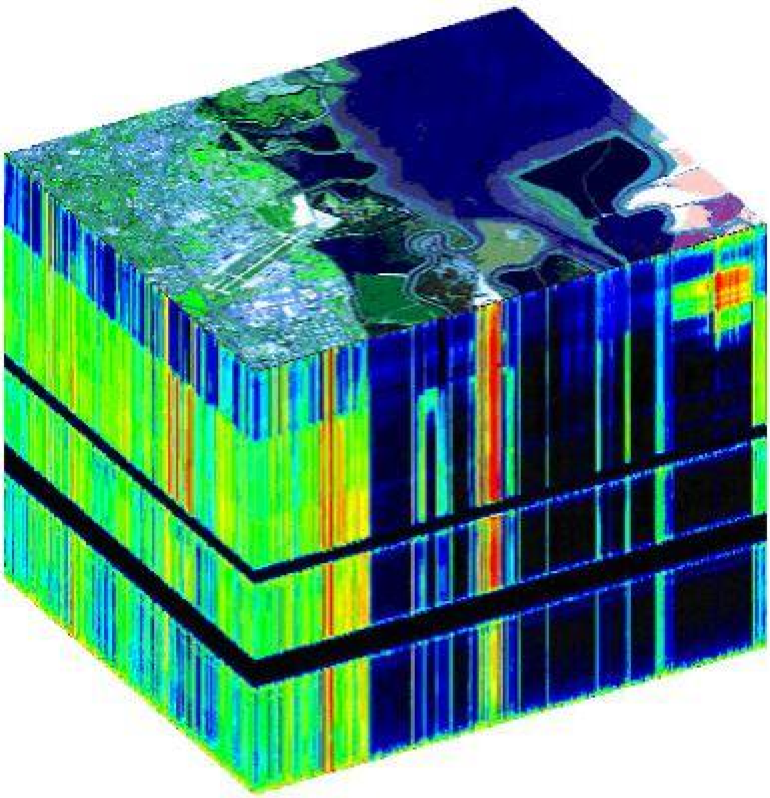

Figure 7: Data Cube Captured by the Hyperspectral Imaging System

Figure 8: Schematic Diagram of UAV Mounting Experiment

1503 Bld. A04, 3rd Software Park, Jimei, Xiamen, 361005, China
Tel: +86-592-6102588

Figure 9: Field Experiment Scene 1 with Optosky Hyperspectral Imaging System

Figure 10: Field Experiment Scene 2 with Optosky Hyperspectral Imaging System

1503 Bld. A04, 3rd Software Park, Jimei, Xiamen, 361005, China
Tel: +86-592-6102588

Figure 11: Field Experiment Scene 3 with Optosky Hyperspectral Imaging System

]

Figure 12: Field Experiment Scene 4 with Optosky Hyperspectral Imaging System

1503 Bld. A04, 3rd Software Park, Jimei, Xiamen, 361005, China
Tel: +86-592-6102588

Figure 13: Field Experiment Scene 5 with Optosky Hyperspectral Imaging System

4.1 Field Vegetation Testing

Our company utilizes a portable ground-based hyperspectral imaging system for spectral data collection across various field objects, including vegetation, tower cranes, and land. Spectral data is displayed, compared, and analyzed based on single-band images and color images. Single-band images reveal distinct differences among various objects at different wavelengths, which can also be observed as differences in the spectral curves. Below are the final spectral curve comparison, single-band images, and color images:

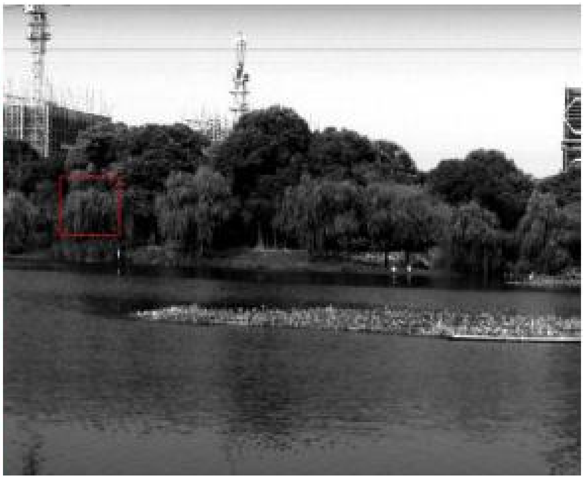

1503 Bld. A04, 3rd Software Park, Jimei, Xiamen, 361005, China
Tel: +86-592-6102588

Figure 14: Hyperspectral Test Imaging in the Field; (a) Image of Band 50; (b) Image of Band 100; (c) Image of Band 200; (d) RGB Composite Image

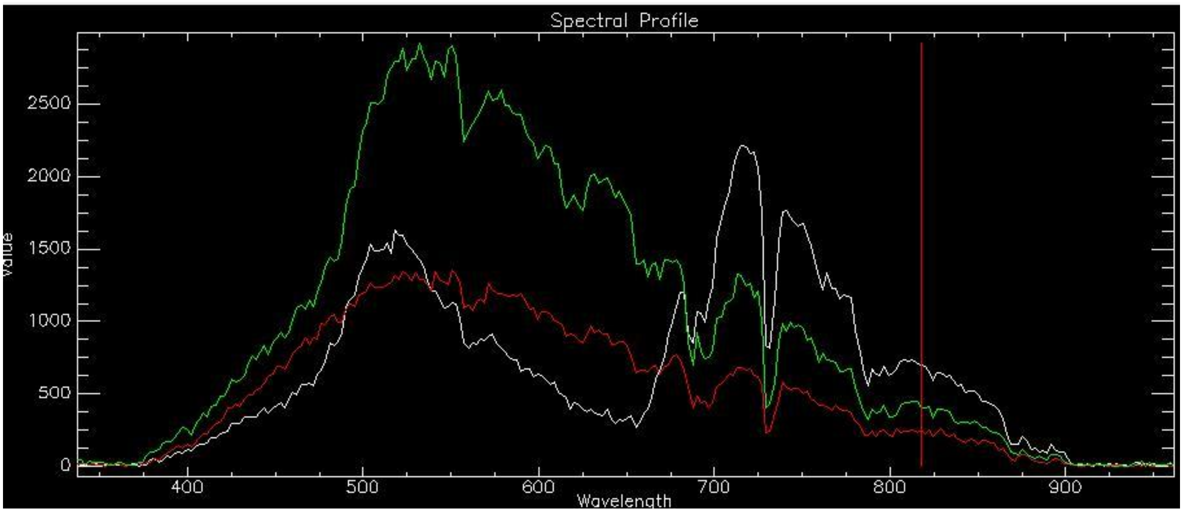

Figure 15: Spectral Curve Comparison

4.2 Archaeological Mural Testing

Currently, hyperspectral imaging is highly suitable for spectral imaging of antiques, murals, oil paintings, and archaeological sites due to its ability to capture the 'fingerprint spectra' of materials. The following images show the real-time results of hyperspectral imaging testing conducted on an ancient mural in a local temple in Sichuan Province, along with the final spectral band data. Our hyperspectral image analysis has accurately and completely restored the colors and condition of the mural, addressing issues such as fading, coverage, and damage. This provides new insights for research on the mural and offers valuable evidence for artifact restoration, authentication, and preservation.

1503 Bld. A04, 3rd Software Park, Jimei, Xiamen, 361005, China
Tel: +86-592-6102588

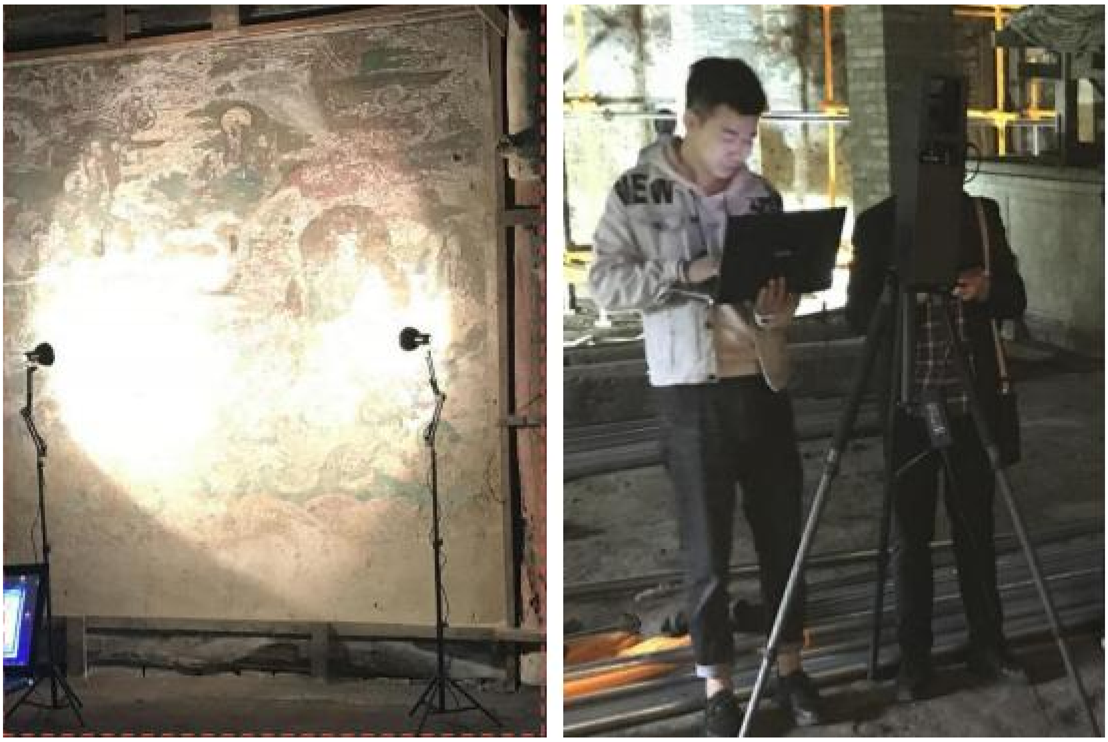

Figure 16: Measurement Real-Time Image

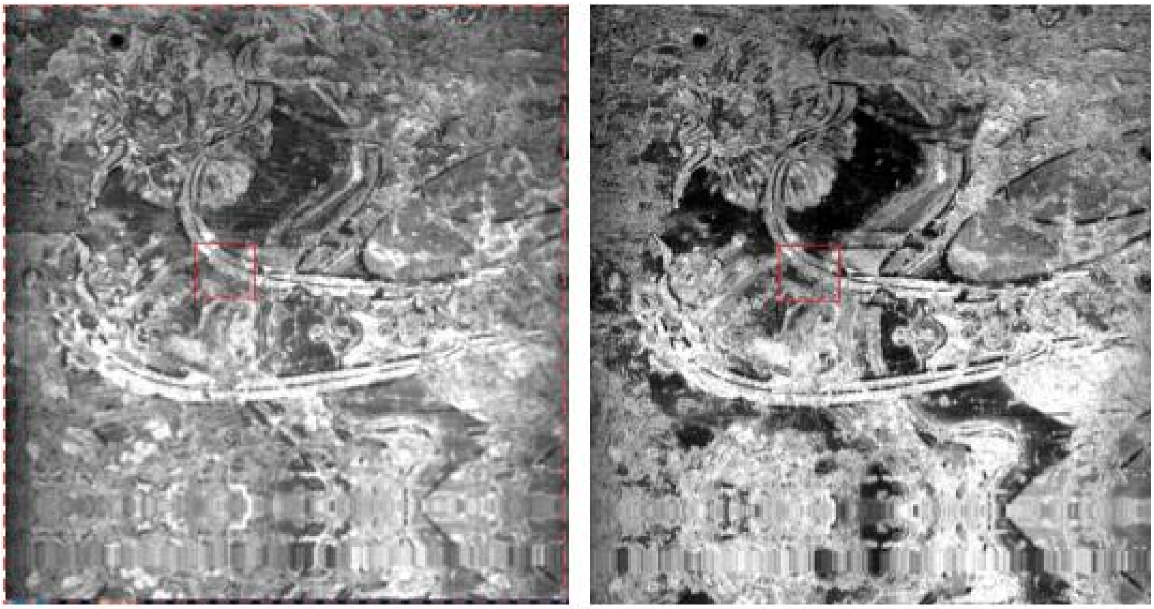

1503 Bld. A04, 3rd Software Park, Jimei, Xiamen, 361005, China
Tel: +86-592-6102588

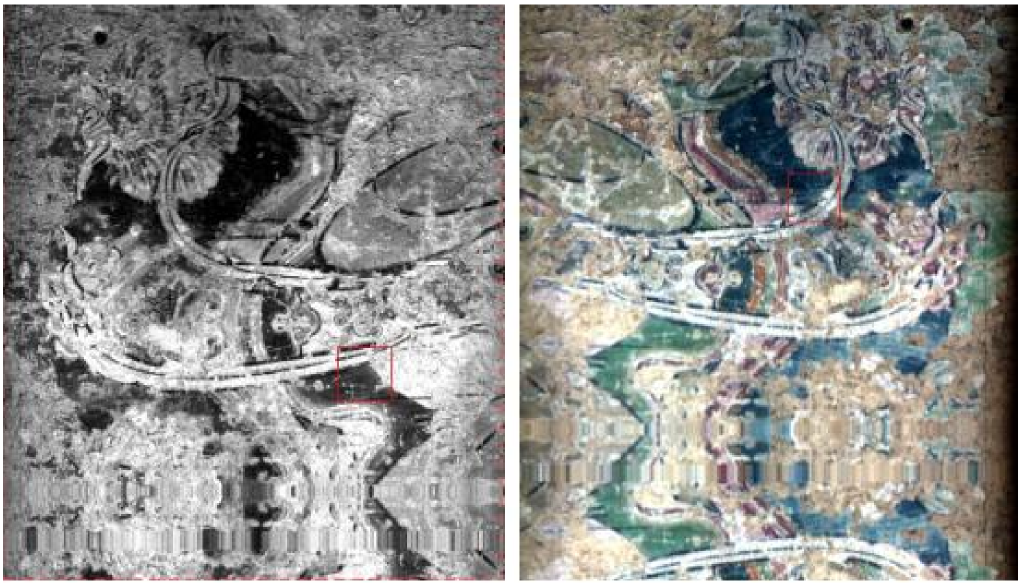

Figure 17: Hyperspectral Imaging of Archaeological Mural; (a) Image of Band 50; (b) Image of Band 150; (c) Image of Band 200; (d) RGB Composite Image

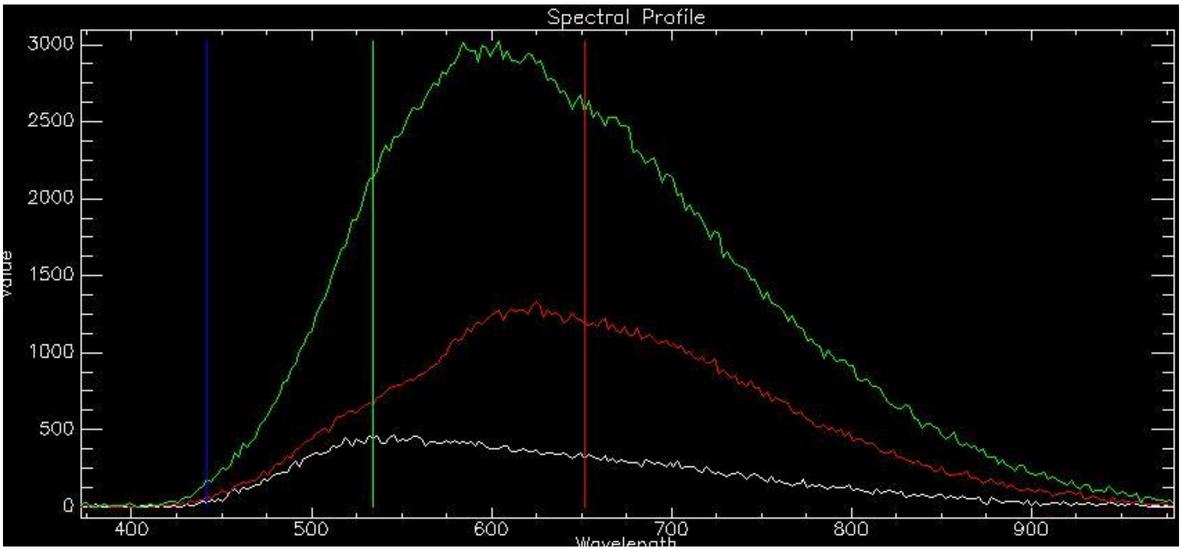

Figure 18: Spectral Image Comparison

4.3 Application in Corn Drought Identification and Classification

Corn is one of the most important staple crops globally and the primary grain crop in China. Northern China is a major corn-producing region, where drought has become a significant factor affecting corn yield due to variations in temperature and precipitation. As the demand for precision agriculture management increases, the accurate and efficient identification of corn drought severity is of great importance.

Traditional methods for identifying crop drought often rely on satellite multispectral remote sensing images to calculate vegetation indices and assess drought conditions. However, factors such as weather, overpass time, and low spatial resolution limit the timeliness and accuracy of satellite imagery. With the advancement of UAV technology, it has become possible to obtain ultra-high-resolution remote sensing images efficiently and flexibly, providing new solutions for

1503 Bld. A04, 3rd Software Park, Jimei, Xiamen, 361005, China
Tel: +86-592-6102588

many agricultural issues in recent years. Furthermore, the development of deep neural networks, particularly the advent of fully convolutional neural networks, has significantly improved the precision of semantic segmentation tasks in remote sensing imagery. Liu Chang from Jilin University utilized the ATP9000 hyperspectral imaging system (now renamed ATH9010) produced by Optosky to design and implement a deep learning-based semantic segmentation method for identifying and classifying corn drought.

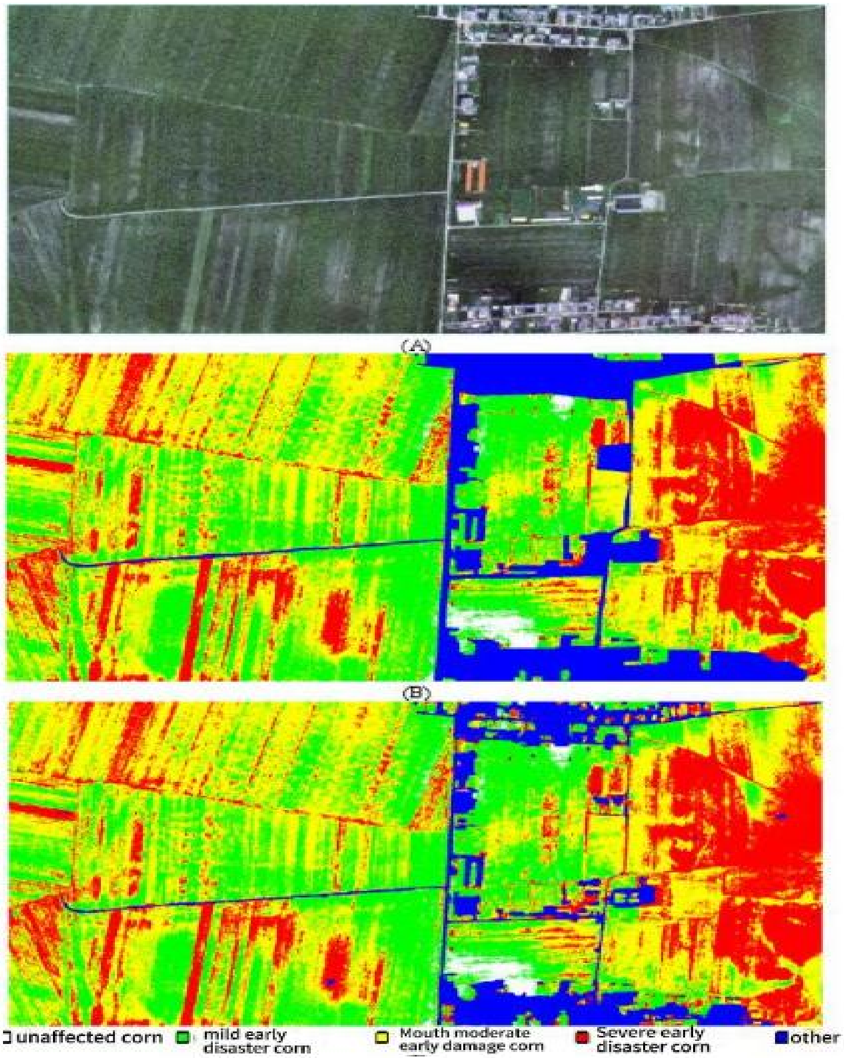

Figure 19: Liu Chang from Jilin University conducted research on corn drought classification using hyperspectral imaging. The study utilized the ATP9000 hyperspectral imaging system (now renamed ATH9010) produced by Optosky.

By applying different algorithms, UAV hyperspectral imaging systems can also survey a variety of more complex types of disasters, such as flooding, pest infestations, and hail damage. These disasters can similarly lead to reduced crop yields and economic losses.

4.4 In Industrial Sorting Applications

With the advancement of near-infrared hyperspectral technology, Jiang et al. have explored using near-infrared hyperspectral technology to detect impurities in cotton. The application of shortwave near-infrared hyperspectral technology has significantly improved the detection rate of plastic films compared to conventional methods. Hyperspectral imaging technology, based on imaging data from numerous narrow bands, provides both image and spectral information of the sample simultaneously. Common hyperspectral data processing methods include Partial Least Squares (PLS), Support Vector Machines (SVM), and Artificial Neural Networks (ANN).

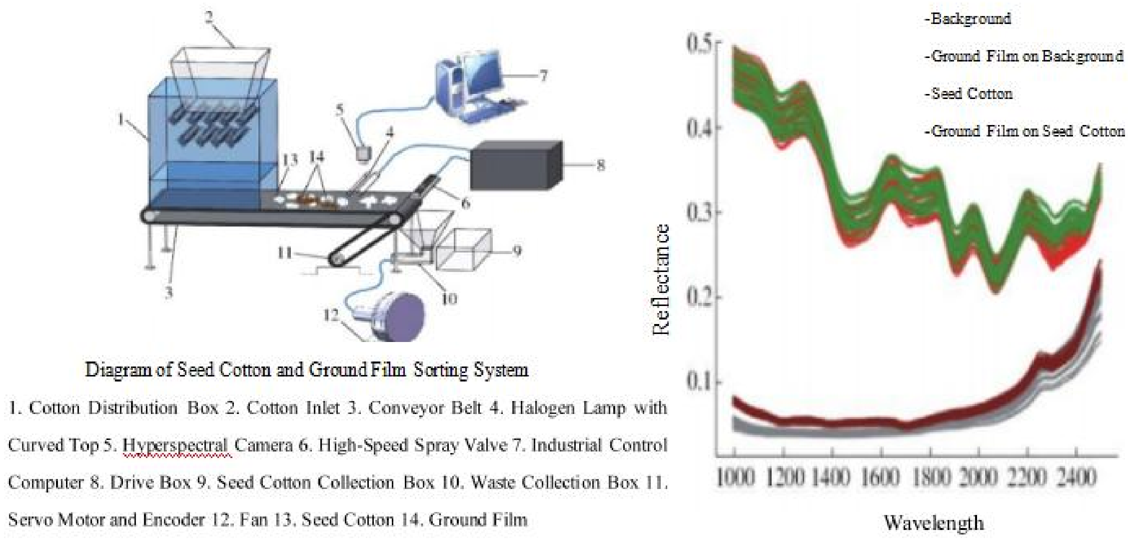

Figure 20: Application of Hyperspectral Imaging System in Seed Cotton Sorting; (a) System Functional Components; (b) Reflectance Spectra Curves of Different Materials

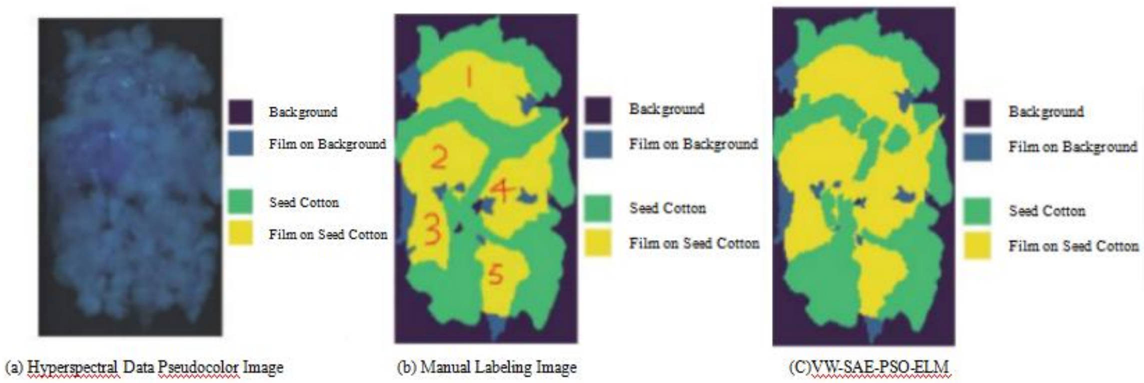

Figure 21: Application of Hyperspectral Imaging System in Seed Cotton Sorting; (a) Manual Labeling; (b) Hyperspectral Imaging System Identification Results

External quality is one of the most intuitive quality characteristics of apples, directly affecting their price and consumer preference. Addressing the challenges and key aspects of external apple detection, this research integrates machine vision technology, hyperspectral imaging technology, and multispectral imaging technology, combining image processing techniques, pattern recognition methods, chemometrics methods, and spectral analysis techniques to study detection methods for external physical quality (shape and size) and common surface defects of apples. The detection system and algorithms developed based on this research lay the foundation for the rapid online quality detection and grading equipment for apples using machine vision technology and multispectral machine vision technology in China.

1503 Bld. A04, 3rd Software Park, Jimei, Xiamen, 361005, China
Tel: +86-592-6102588

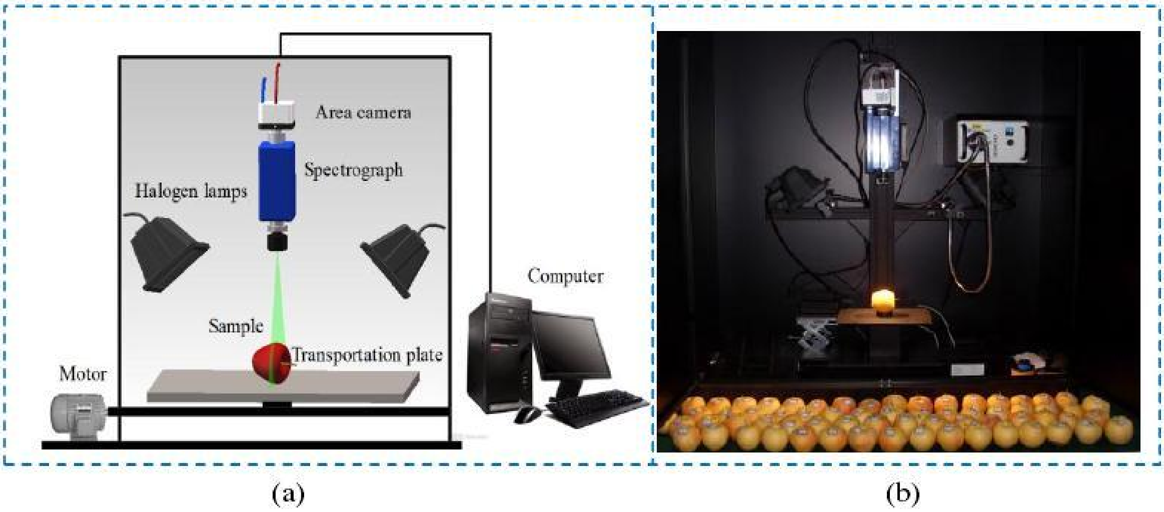

Figure 22: Principle Diagram and Actual Image of the Hyperspectral Imaging System Developed by Dr. Zhang Baohua from Shanghai Jiao Tong University; (a) Principle Diagram; (b) Actual Image

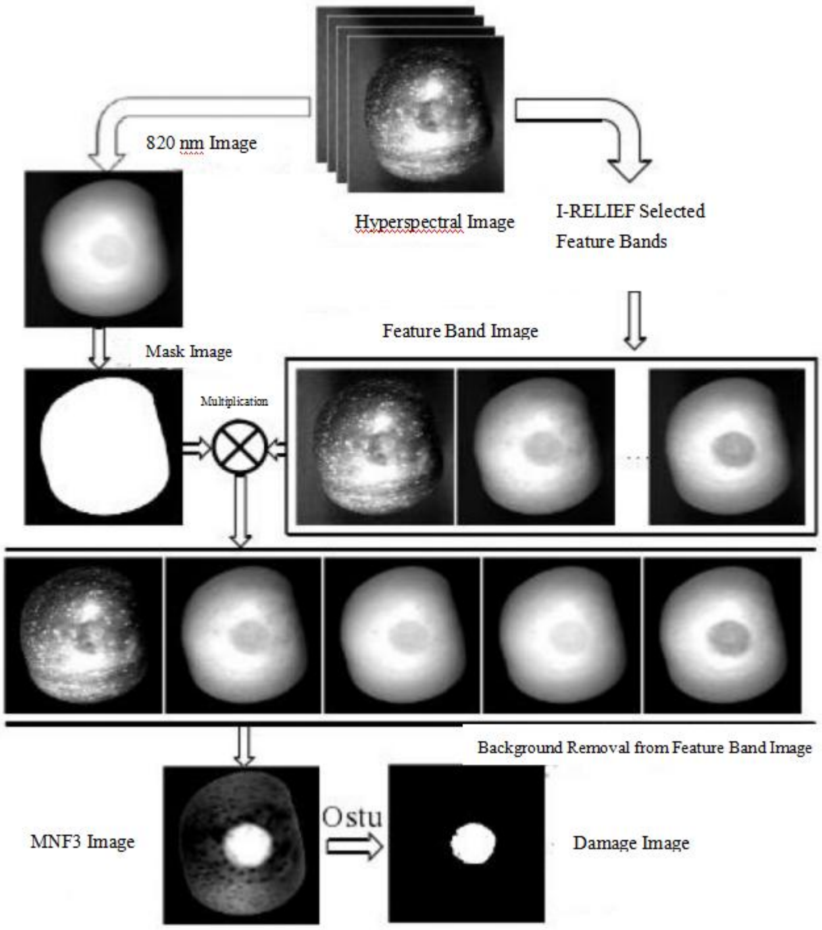

Figure 23: Flowchart of Early Surface Damage Detection Algorithm for Apples

1503 Bld. A04, 3rd Software Park, Jimei, Xiamen, 361005, China
Tel: +86-592-6102588

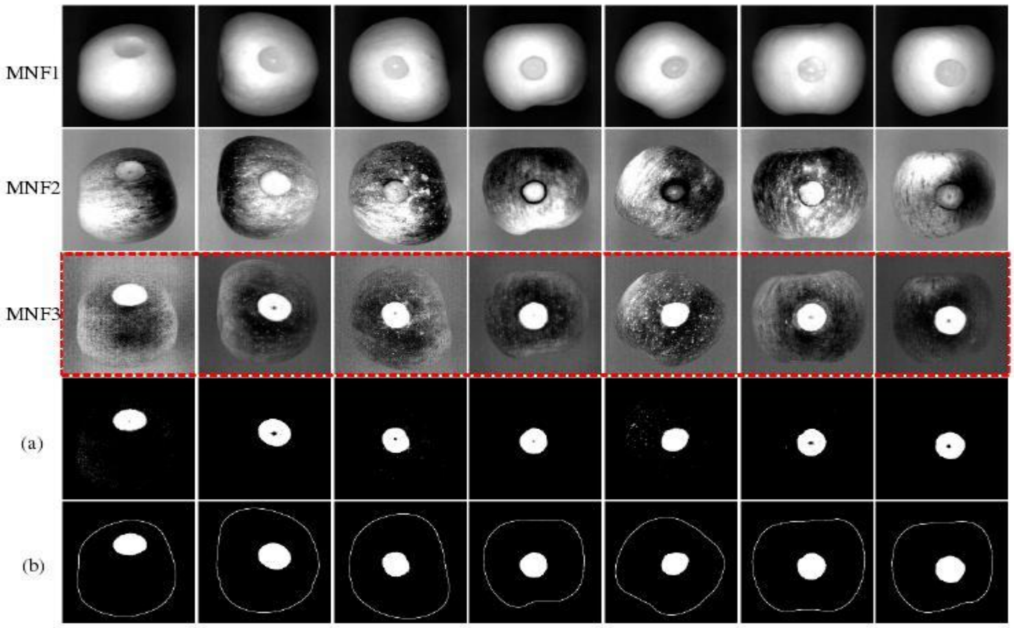

Figure 24: Identification Results and Intermediate Processing of Early Apple Rot; (a) Rot Segmentation Results; (b) Final Results

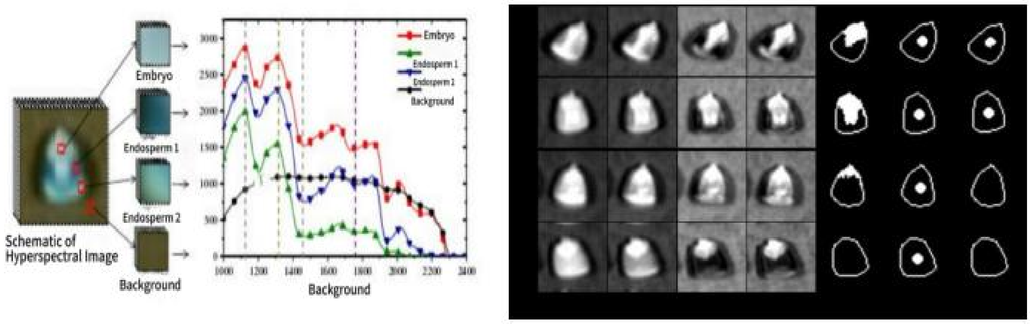

Figure 25: Application of 1000-2500 nm Hyperspectral Imaging System in Corn Seed Sorting (Dr. Wang Chaopeng, Northwest A&F University)

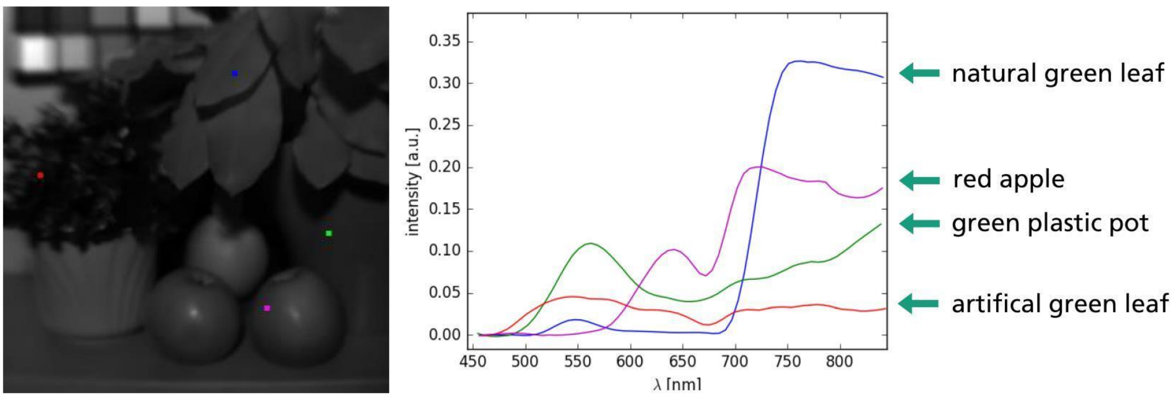

Figure 26: Spectra of Natural Green Plants, Artificial Green Leaves, Green Plastic, and Red Apples

1503 Bld. A04, 3rd Software Park, Jimei, Xiamen, 361005, China
Tel: +86-592-6102588

4.5 Application in Precision Agriculture

Figure 27: UAV Hyperspectral Remote Sensing System Produced by Optosky

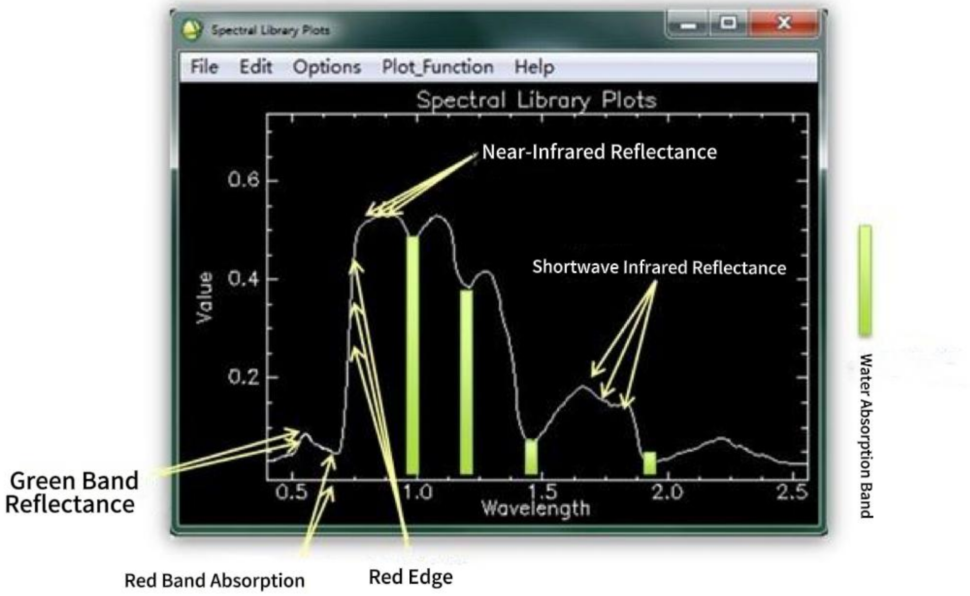

Figure 28: Spectral Image of Green Plants Measured by Hyperspectral Imaging System

(1) Crop Growth Monitoring and Yield Estimation: Throughout different growth stages, crops exhibit variations in internal composition and external morphology due to external factors, with leaf area index being a key indicator. Leaf area index reflects both individual and collective characteristics of crop growth.

(2) Pest and Disease Control: Remote sensing technology can monitor the impact of pests and diseases on crop growth and development, track crop growth conditions, estimate disaster losses, and monitor pest distribution and behavior, aiding in pest prevention.

(3) Drought Monitoring: Remote sensing technology monitors crop drought conditions using vegetation indices and canopy parameters.

(4) Soil Moisture Content and Distribution Monitoring: Under varying thermal inertia conditions, differences in remote sensing spectra are significant. By establishing a mathematical model

between thermal inertia and soil moisture content, remote sensing technology utilizes this model to analyze soil moisture content and distribution.

(5) Crop Nutrient Monitoring: Remote sensing technology offers high precision in monitoring nitrogen content in crops compared to other nutrients. By using single bands and any two bands within the 450 – 882 nm range to construct normalized difference spectral index (NDSI), ratio spectral index (RSI), and simple spectral index (SSI), the correlation between CGI (Crop Growth Index) and spectral indices is calculated. Relevant spectral indices are selected based on their correlation, and an inversion model is established using Partial Least Squares Regression (PLSR). Using CGI as the indicator, UAV hyperspectral imaging is applied for monitoring wheat growth across multiple developmental stages in 2015. The UAV hyperspectral imaging provides accurate CGI inversion, allowing for the assessment of overall wheat growth variations and offering valuable reference for monitoring wheat growth.

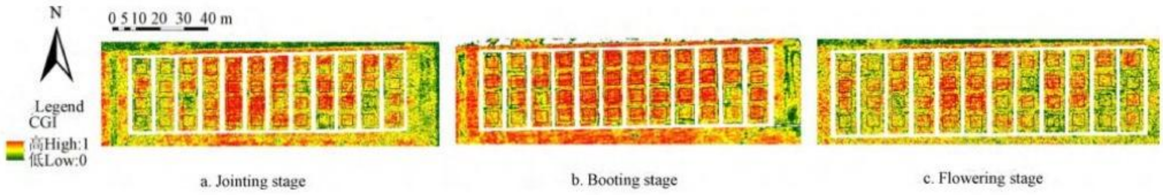

Figure 29: CGI Inversion of Wheat Growth Indicator

4.6 Application in Forest Health Assessment

Used for Pest and Disease Monitoring, Forest Resource Assessment；

The health status of vegetation is related to greenness index, leaf area index, leaf moisture content, and light use efficiency；

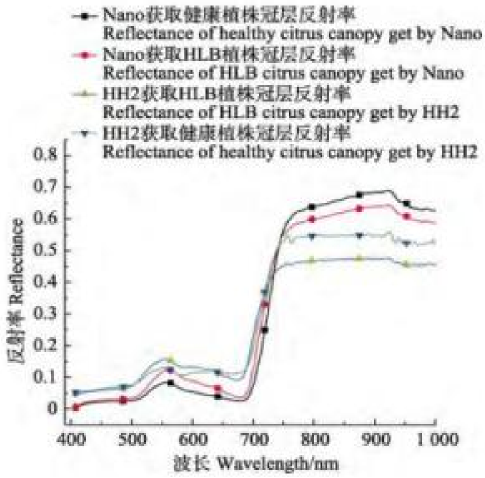

1503 Bld. A04, 3rd Software Park, Jimei, Xiamen, 361005, China
Tel: +86-592-6102588

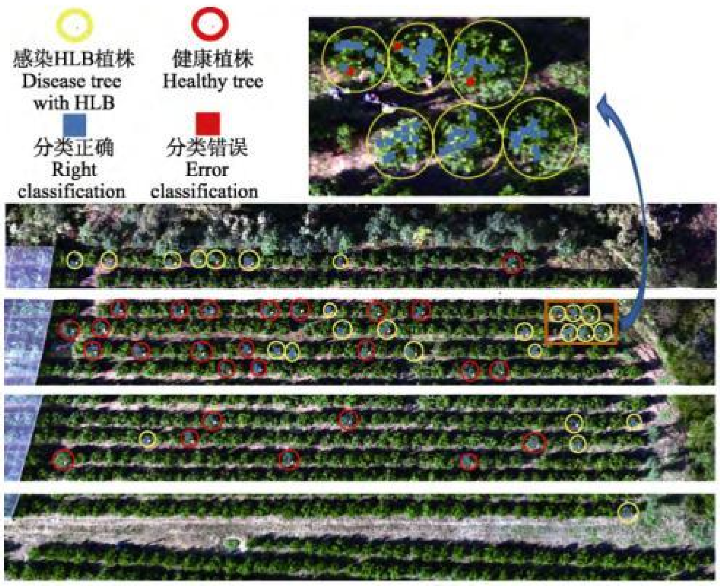

Figure 30: Monitoring and Classification of Citrus Huanglongbing-Infected Plants Using UAV Hyperspectral Remote Sensing (Designed by Lan Yubin et al., South China Agricultural University)

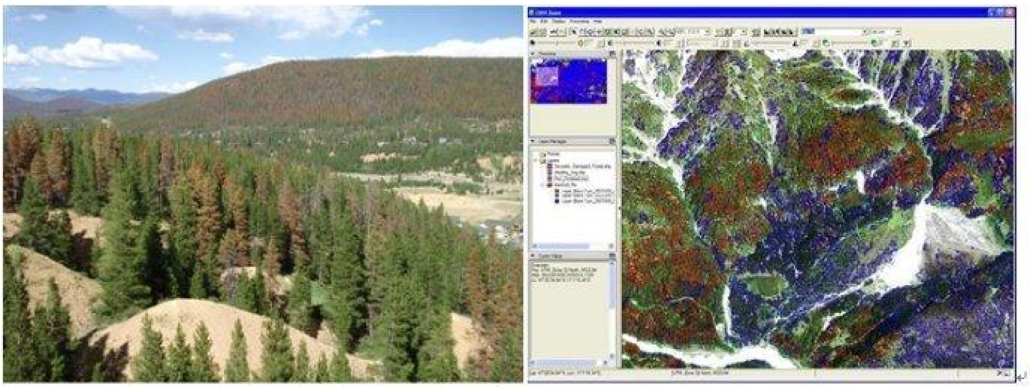

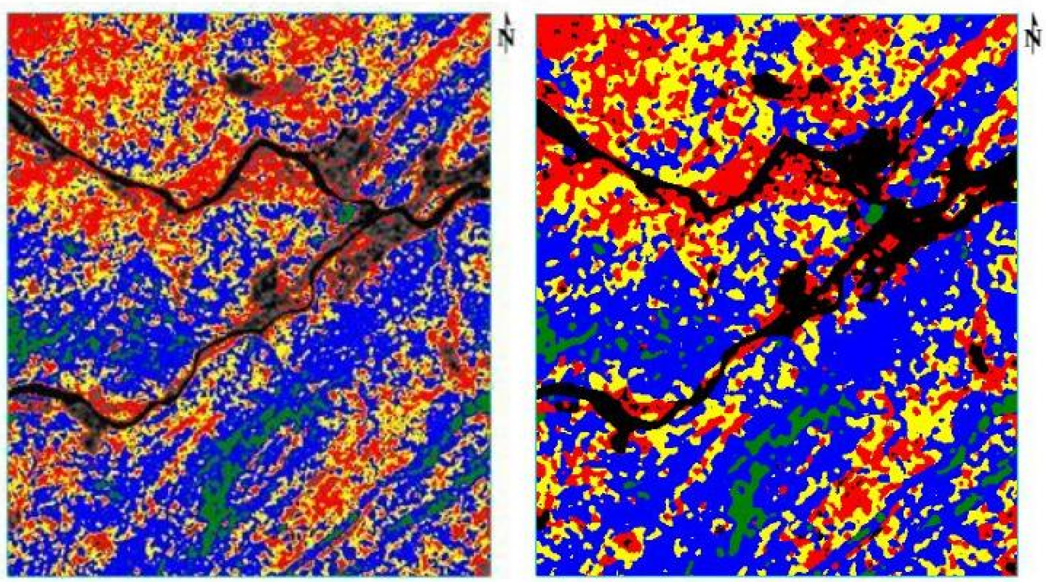

1503 Bld. A04, 3rd Software Park, Jimei, Xiamen, 361005, China
Tel: +86-592-6102588

Figure 31: Distribution Map of Pinus massoniana Health Levels Studied Using Hyperspectral Imaging by Wang Shuang, University of Electronic Science and Technology of China

Spectral remote sensing technology evolved from multispectral remote sensing technology, represented by Landsat, and began to take shape in the mid-1980s (Goetsch et al., 1985; Tong Qingxi et al., 2006). With its high spectral resolution and integrated spectral data advantages, hyperspectral remote sensing technology can finely detect and analyze surface rock and mineral components on a large spatial scale. It not only provides macro images of the surface but also determines mineral types, abundances, and even the chemical composition of certain minerals at the pixel level (Wang Runsheng et al., 2010). In recent years, with the continued development of hardware, data processing methods, and software related to imaging spectrometers, the application of hyperspectral remote sensing technology in geological surveys has accelerated. From large metallogenic belts to medium-sized mineral fields, hyperspectral remote sensing technology plays a crucial role in geological mapping, delineation of hydrothermal alteration zones, and identification and classification of mineralization anomalies (e.g., Bierwirth et al., 2002; Lian Changyun et al., 2005; Kruse et al., 2006; Cudahy et al., 2007; Wang Runsheng et al., 2010; Liu Dechang et al., 2011; Yan Baikun et al., 2014; Yang Zian et al., 2015; Graham et al., 2017). As the metallogenic system theory (Wyborn et al., 1994) becomes more deeply integrated into exploration practices, thematic mineral mapping on a large scale in mineral-rich areas and metallogenic belts will provide critical regional compositional information for predictive exploration.

The spectral wavelength ranges used for mineral mapping include visible light (400 – 700 nm), near-infrared (700 – 1000 nm), shortwave infrared (1000 – 2500 nm), and thermal infrared (7000 – 15000 nm). Currently, the most widely used range in mining applications is the shortwave infrared region (1000 – 2500 nm). This is because the frequencies within the shortwave infrared range are close to the vibrational frequencies of chemical bonds in mineral lattices. Consequently, it is possible to observe minerals containing water or OH- (mainly layered silicates and clay minerals) as well as certain sulfates and carbonates in this wavelength range.

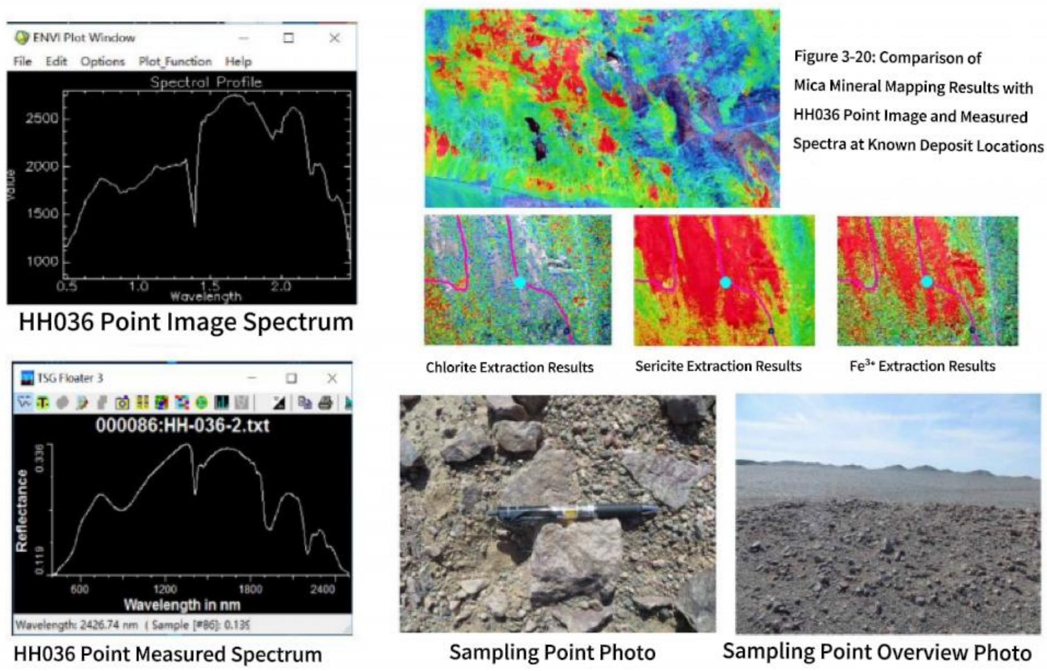

Figure 3-20: Comparison of Mica Mineral Mapping Results with HH036 Point Image and Measured Spectra at Known Deposit Locations

1503 Bld. A04, 3rd Software Park, Jimei, Xiamen, 361005, China
Tel: +86-592-6102588

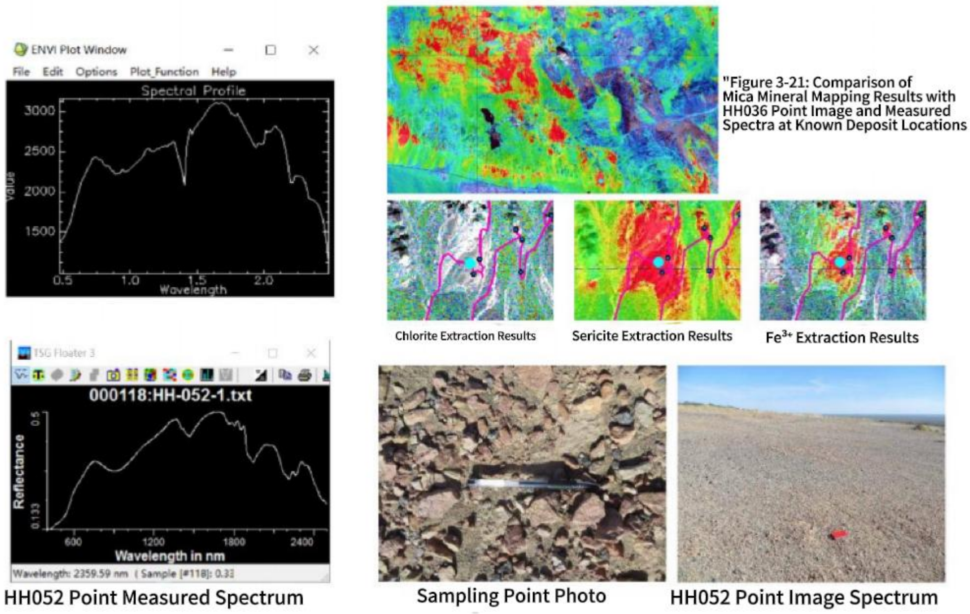

Figure 32: Application of Hyperspectral Imaging in Mineral Exploration

Soil salinization is a significant ecological and environmental issue in arid and semi-arid regions. The consequences of soil salinization, such as soil hardening, decreased fertility, pH imbalance, and land degradation, severely constrain agricultural development and impact China's current sustainable development strategy. Remote sensing technology, with its large scale, broad coverage, timeliness, and cost-effectiveness, effectively addresses the limitations of traditional salinization monitoring methods and provides a new approach for the quantitative monitoring of soil salinization.

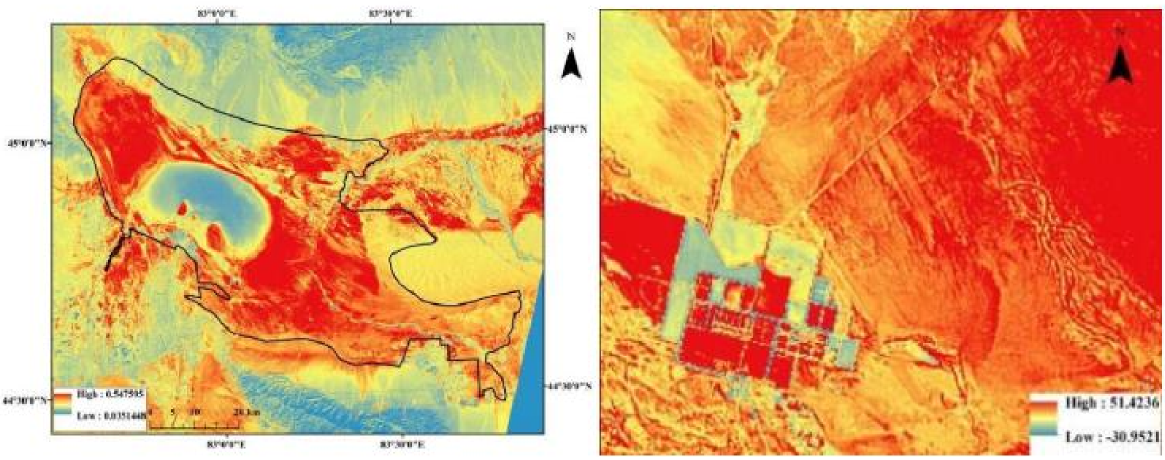

Figure 33: Surrounding Area of a Salt Field

1503 Bld. A04, 3rd Software Park, Jimei, Xiamen, 361005, China
Tel: +86-592-6102588

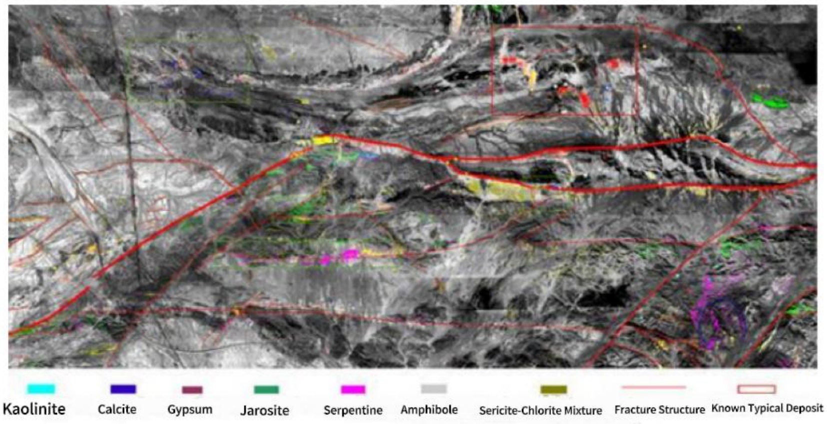

Figure 34: Measurement Map of a Mining Site

4.8 Applications in Public Safety

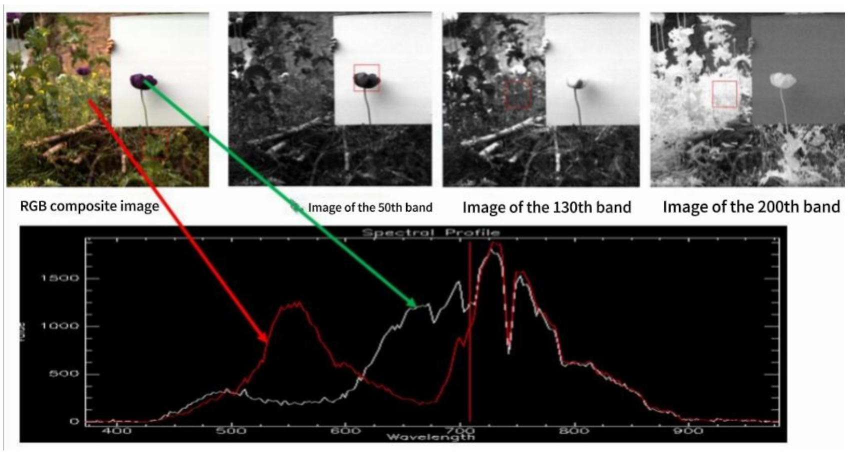

Figure 35: Application of Hyperspectral Imaging in Detecting Illegal Poppy Cultivation

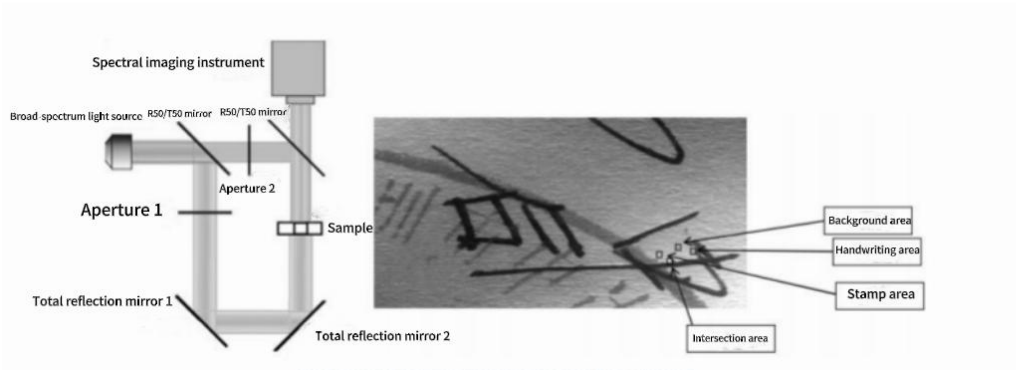

Figure 36: Application of Hyperspectral Imaging in Document Examination

1503 Bld. A04, 3rd Software Park, Jimei, Xiamen, 361005, China
Tel: +86-592-6102588

4.9 Medical Microscopy Spectral Imaging Applications

Application Objective: Intraoperative Online Detection and Navigation for Tumor Surgery

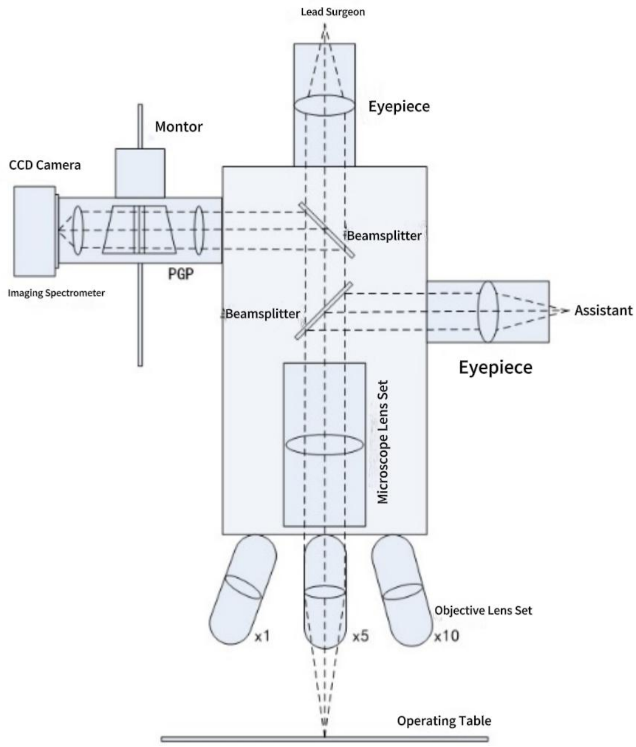

Figure 37: Schematic Diagram of the Optical Path of a Medical Microscopy Spectral Imaging System

The diagram shows the principle of a medical microscopy spectral imaging system. The target on the operating table is divided into three paths after passing through the objective lens and microscope lens system: one path is for direct visual observation by the main surgeon, another for auxiliary visual observation by the assistant, and the third path is for detection and reception by the imaging spectrometer. The imaging spectrometer, driven by a motor, performs spatial scanning of the target, acquiring the imaging spectral information. After data analysis and image processing, the results are displayed to the surgeon on a monitor.

1503 Bld. A04, 3rd Software Park, Jimei, Xiamen, 361005, China
Tel: +86-592-6102588

Figure 38: Photo of the Medical Microscopy Spectral Imaging System

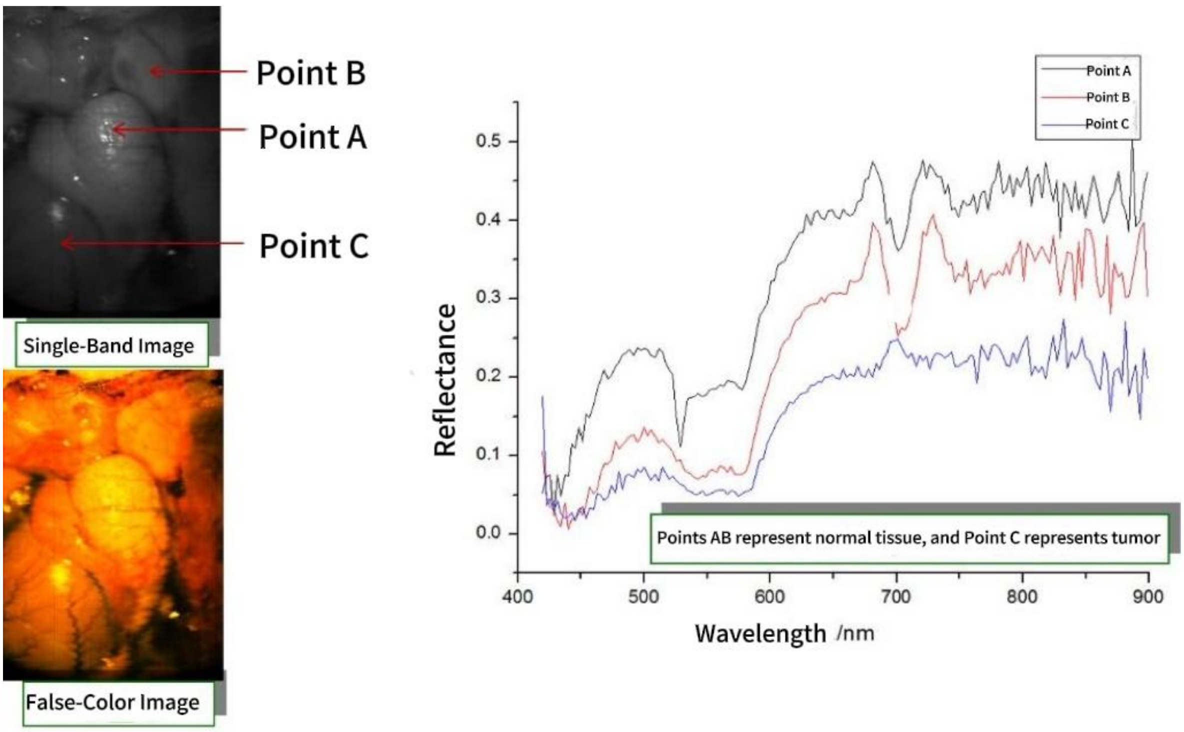

Figure 39: Data from the Medical Microscopy Spectral Imaging System

1503 Bld. A04, 3rd Software Park, Jimei, Xiamen, 361005, China
Tel: +86-592-6102588

4.10 Applications of Airborne Imaging Spectroscopy

Figure 40: ATH9010 Airborne Hyperspectral Imaging System Produced by Optosky

Figure 41: ATH9010NY-FW Fixed-Wing Drone Crop Inspection System

1503 Bld. A04, 3rd Software Park, Jimei, Xiamen, 361005, China
Tel: +86-592-6102588

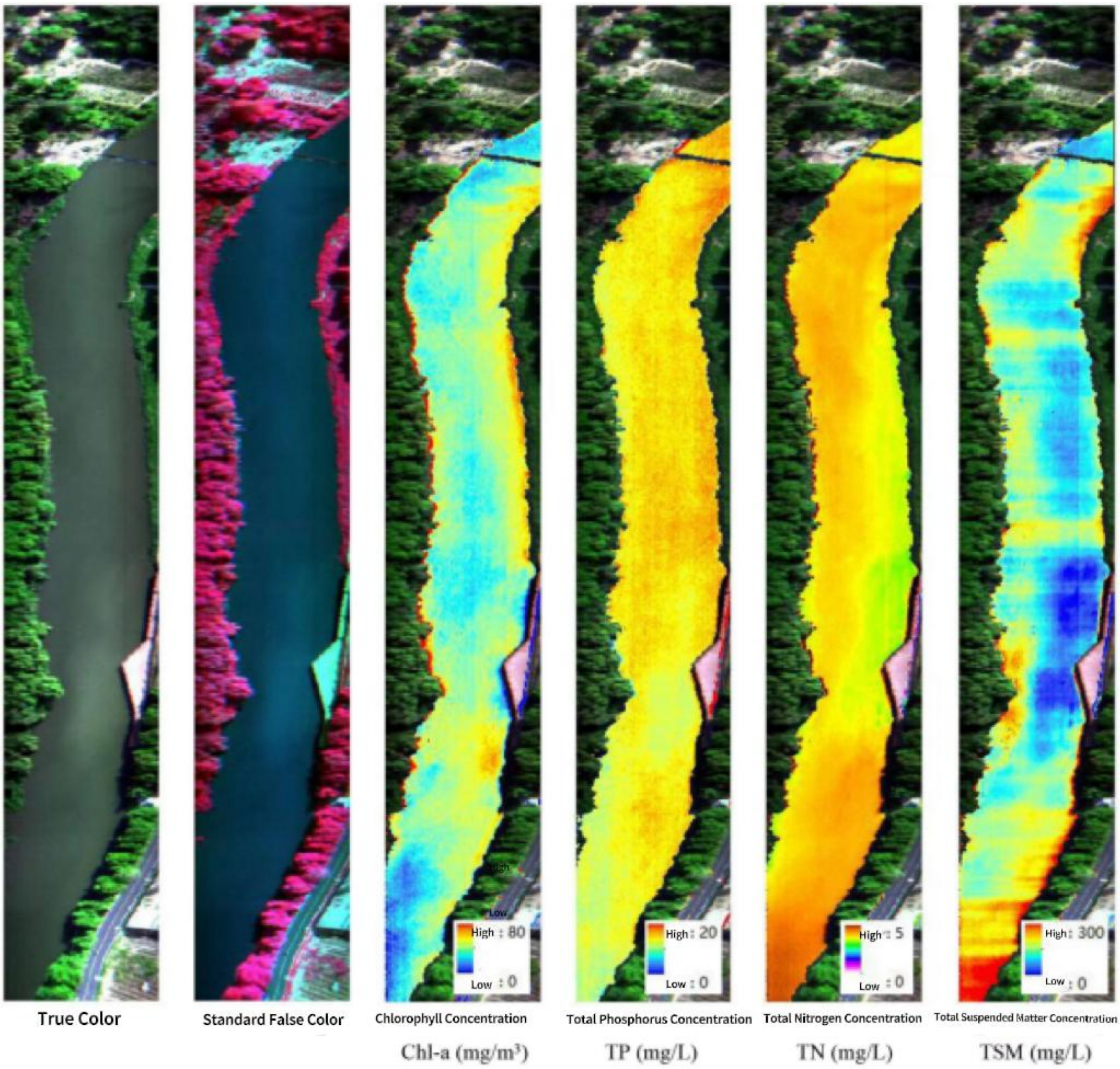

Figure 42: River Water Quality Monitoring Data Inversion Results from ATH9010 Hyperspectral Drone (Flight Location: Xiamen, Fujian Province; Flight Altitude: 100m; Airspeed: 6m/s; Wind Speed: Level 2)

1503 Bld. A04, 3rd Software Park, Jimei, Xiamen, 361005, China
Tel: +86-592-6102588

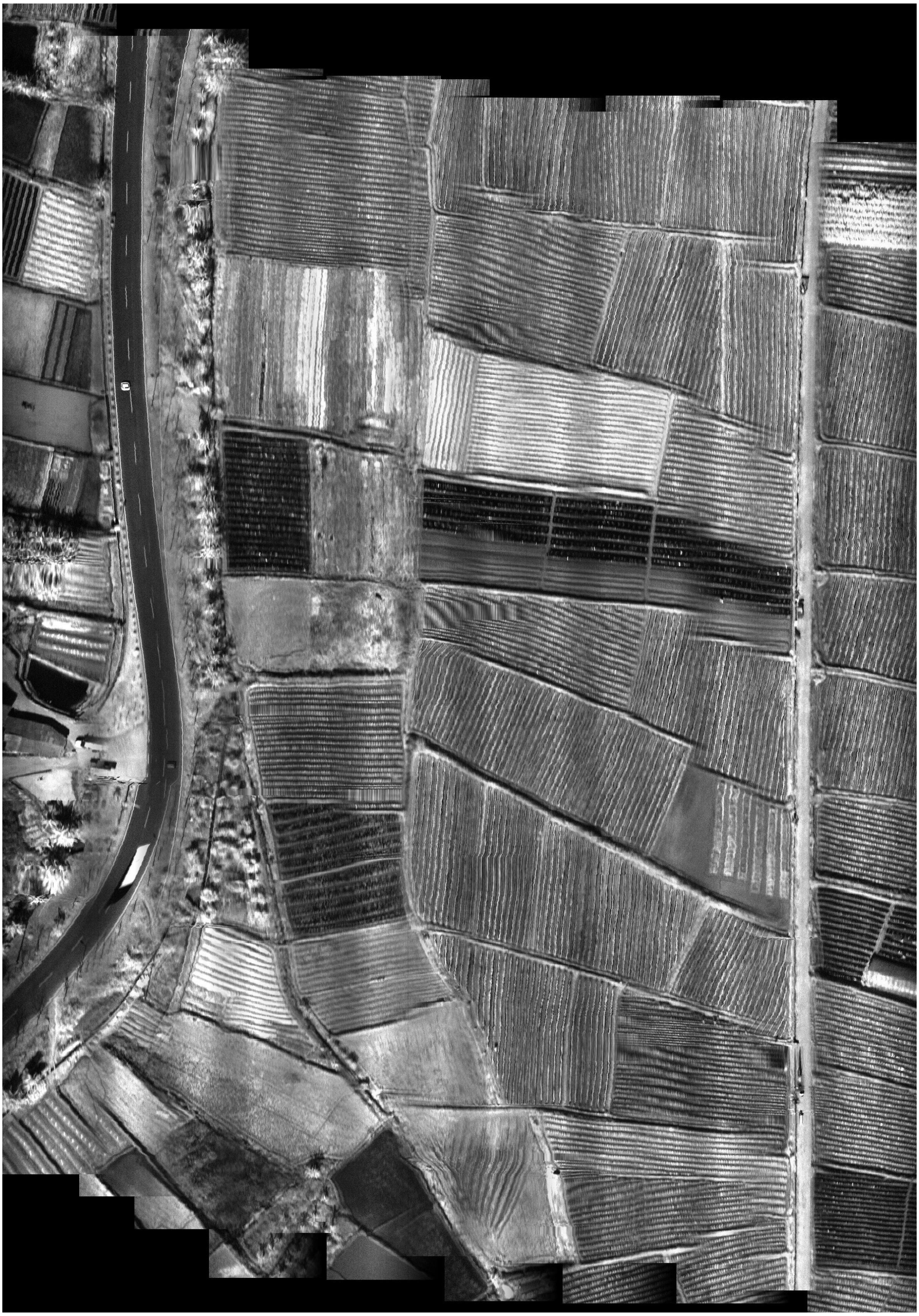

Figure 43: Large-Area Tobacco Planting Multi-Flight Strip Hyperspectral Stitching Data from ATH9010 Hyperspectral Drone (Flight Location: Changting County, Longyan City, Fujian Province; Flight Altitude: 100m; Airspeed: 6m/s; Wind Speed: Level 3)

1503 Bld. A04, 3rd Software Park, Jimei, Xiamen, 361005, China
Tel: +86-592-6102588

Application Goal: Airborne Remote Sensing

High-spectral remote sensing sensors can accurately monitor the biochemical parameters of crops. For example, experiments can be designed for different sowing periods of rice, cotton, maize, and wheat, using high-spectral remote sensing sensors to obtain biochemical and corresponding hyperspectral reflectance data at various growth stages. By analyzing the hyperspectral reflectance characteristics and their relationship with biochemical parameters at different growth stages, sensitive spectral bands that reflect biochemical parameters can be determined. Extracting these sensitive bands for different biochemical parameters through hyperspectral remote sensing sensors will aid in exploring monitoring methods and developing mathematical models for estimating these parameters. The development and application of hyperspectral remote sensing sensors will be a significant direction in the advancement of remote sensing technology.

1503 Bld. A04, 3rd Software Park, Jimei, Xiamen, 361005, China
Tel: +86-592-6102588

1) Crop Growth Monitoring and Yield Prediction

During different growth stages of crops, variations in internal composition and external morphology occur due to external factors, with the leaf area index being the most notable difference. The leaf area index is a comprehensive indicator reflecting both individual and collective characteristics of crop growth. Remote sensing technology enables the analysis of leaf area index at different crop growth stages by periodically capturing the electromagnetic spectrum emitted by the crops, thus monitoring crop growth and predicting yield. In 2009, the Heilongjiang River Farm in Inner Mongolia used remote sensing technology to measure the barley leaf area index to determine its growth status. In 2010, the 852 Farm in Heilongjiang used remote sensing technology to map the spatial distribution of rice quality to predict rice yield. In the 1980s, the United States employed remote sensing technology to estimate wheat planting areas and yields.

Figure 44 Crop growth status (i.e., yield assessment) survey map. Areas with deeper green indicate better growth and higher yield.

1503 Bld. A04, 3rd Software Park, Jimei, Xiamen, 361005, China
Tel: +86-592-6102588

2) Crop Pest and Disease Control

Remote sensing technology can monitor the impact of pests and diseases on crop growth and development, track the crop's development status, estimate damage losses, and monitor pest distribution and behavior. This enables effective pest prevention. In 2010, the Qianjin Farm in Heilongjiang used remote sensing technology to map and monitor rice blast disease to prevent pest and disease outbreaks.

In the early stages of crop pests and diseases, although the leaf structure may have changed, this change can be accurately detected through near-infrared spectral reflectance. However, the quantity and quality of chlorophyll in the crops may not have significantly changed, so visible light spectral reflectance will not show noticeable differences and is difficult for the human eye to observe. Infrared remote sensing technology can provide timely and accurate predictions, distinguishing the extent of crop damage and preventing the spread of pests and diseases. For example, using near-infrared wavelengths in the range of 0.7 - 0.9 μm can accurately detect black rust disease in wheat and oats.

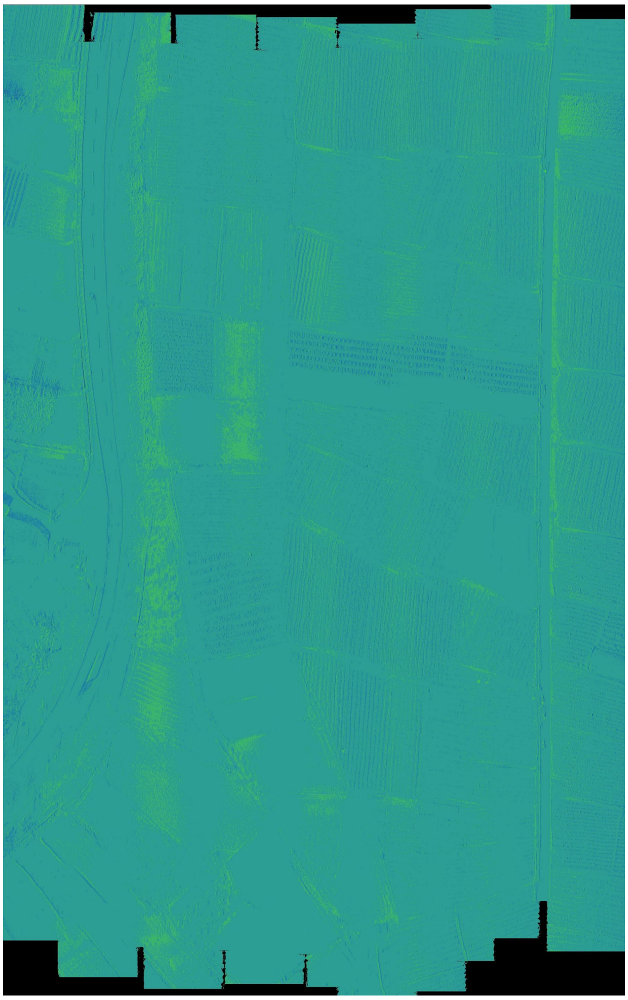

Figure 45. Crop Pest and Disease Surveillance Map. Light green areas indicate suspected pest and disease outbreak zones.

1503 Bld. A04, 3rd Software Park, Jimei, Xiamen, 361005, China
Tel: +86-592-6102588

3) Crop Drought Monitoring

During dry weather conditions, insufficient water absorption by crops affects their growth and development, leading to a decrease in vegetation indices. Without adequate water supply, crops experience inhibited aerobic respiration, forcing leaf stomata to partially close, thereby causing an increase in canopy temperature. Remote sensing technology monitors crop drought conditions through vegetation indices and canopy parameters.

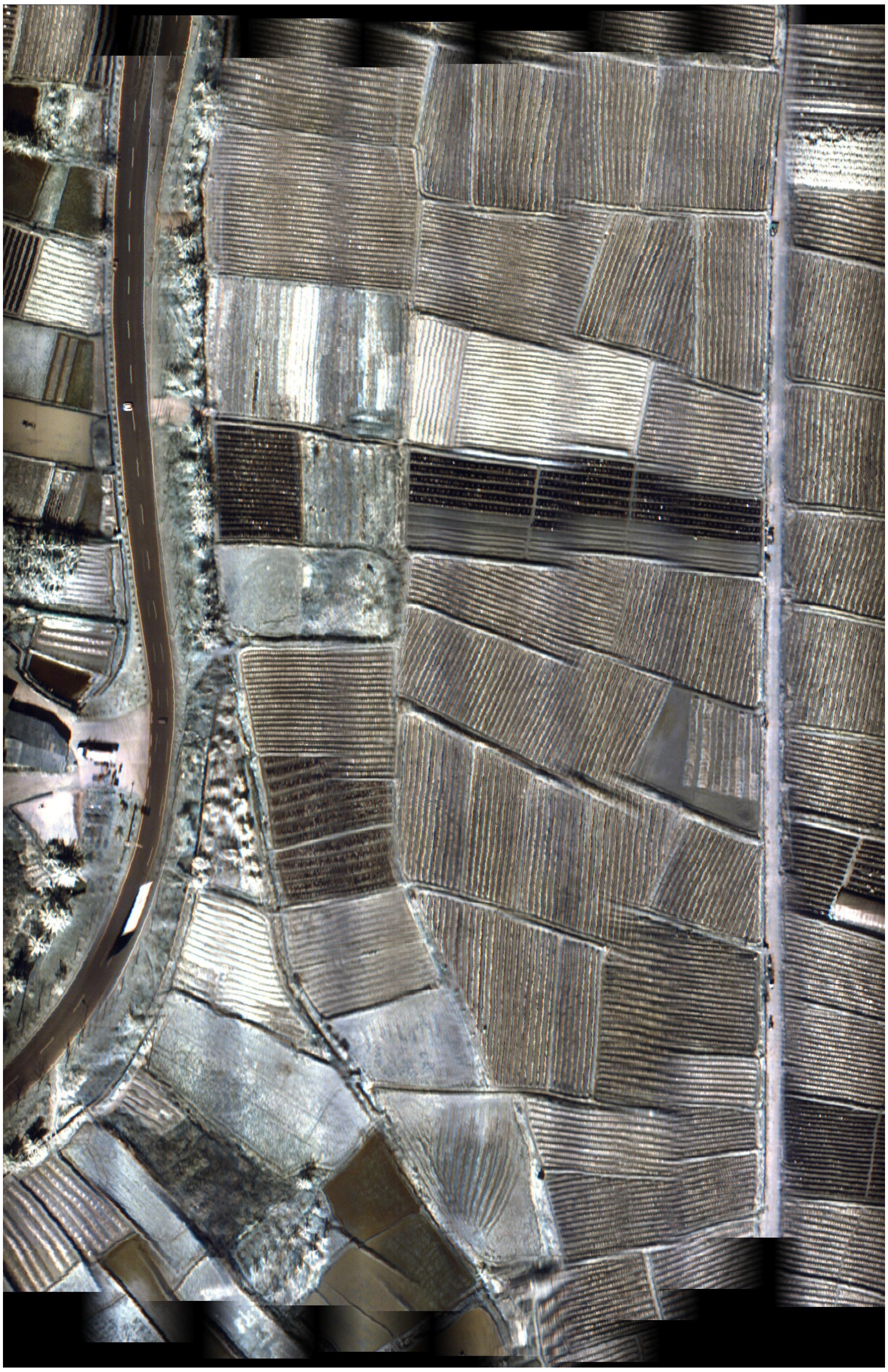

Figure 46. Drought situation map, the dark colored areas are water shortage areas

4) Plant Yield Assessment

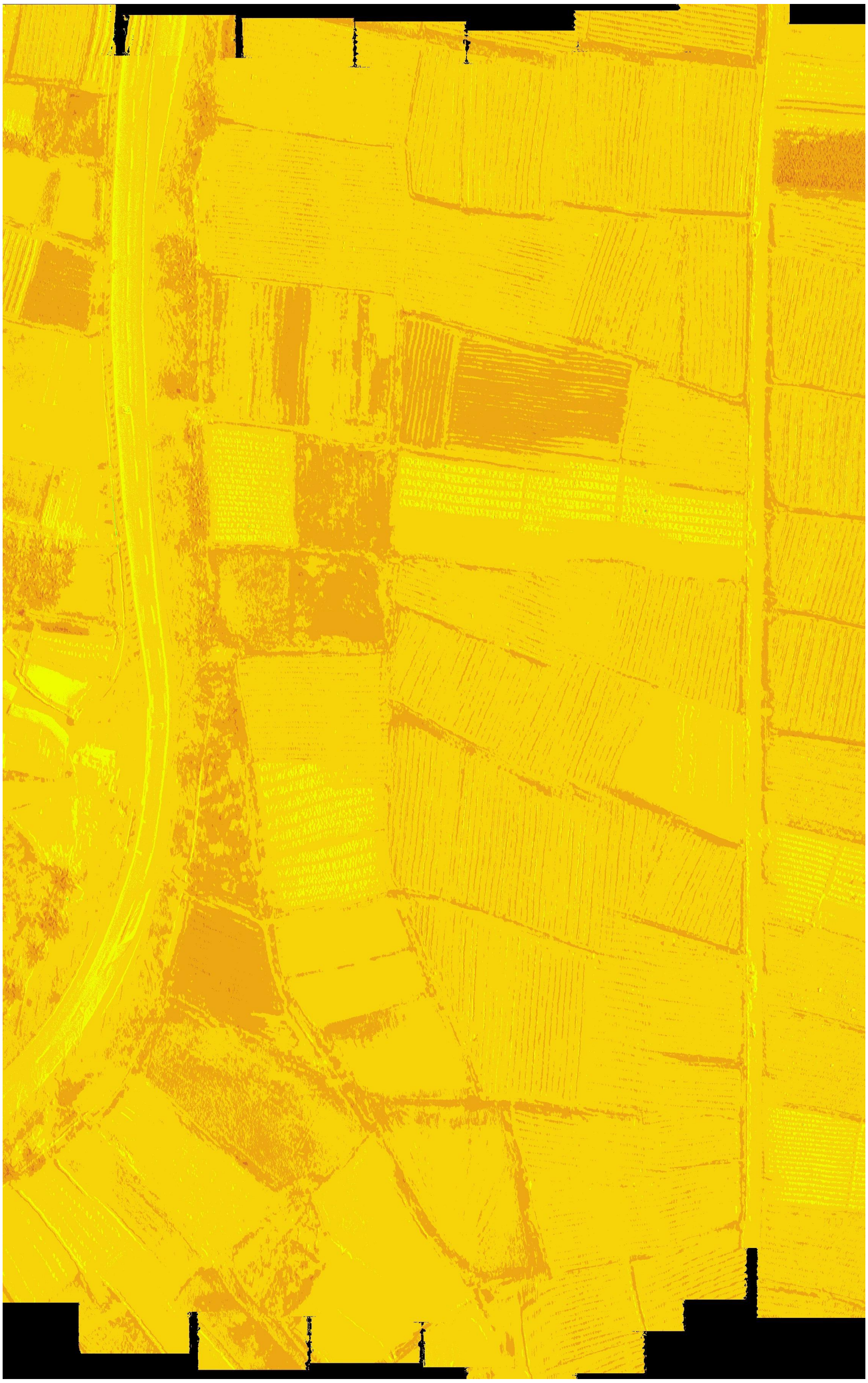

Figure 47. Plant vegetation health monitoring and yield evaluation. The darker the yellow color, the healthier the plant and the higher the yield.

1503 Bld. A04, 3rd Software Park, Jimei, Xiamen, 361005, China
Tel: +86-592-6102588

5) Crop nutrient monitoring

The nutrient content of crops directly affects the chlorophyll content of crop leaves. A mathematical model is established between the vegetation index and different nutrients (such as nitrogen, phosphorus, potassium, calcium, magnesium, etc.) to predict the supply of crop nutrients. . According to a large number of experimental studies, remote sensing technology can detect nitrogen content in crops with higher accuracy than other nutrients.

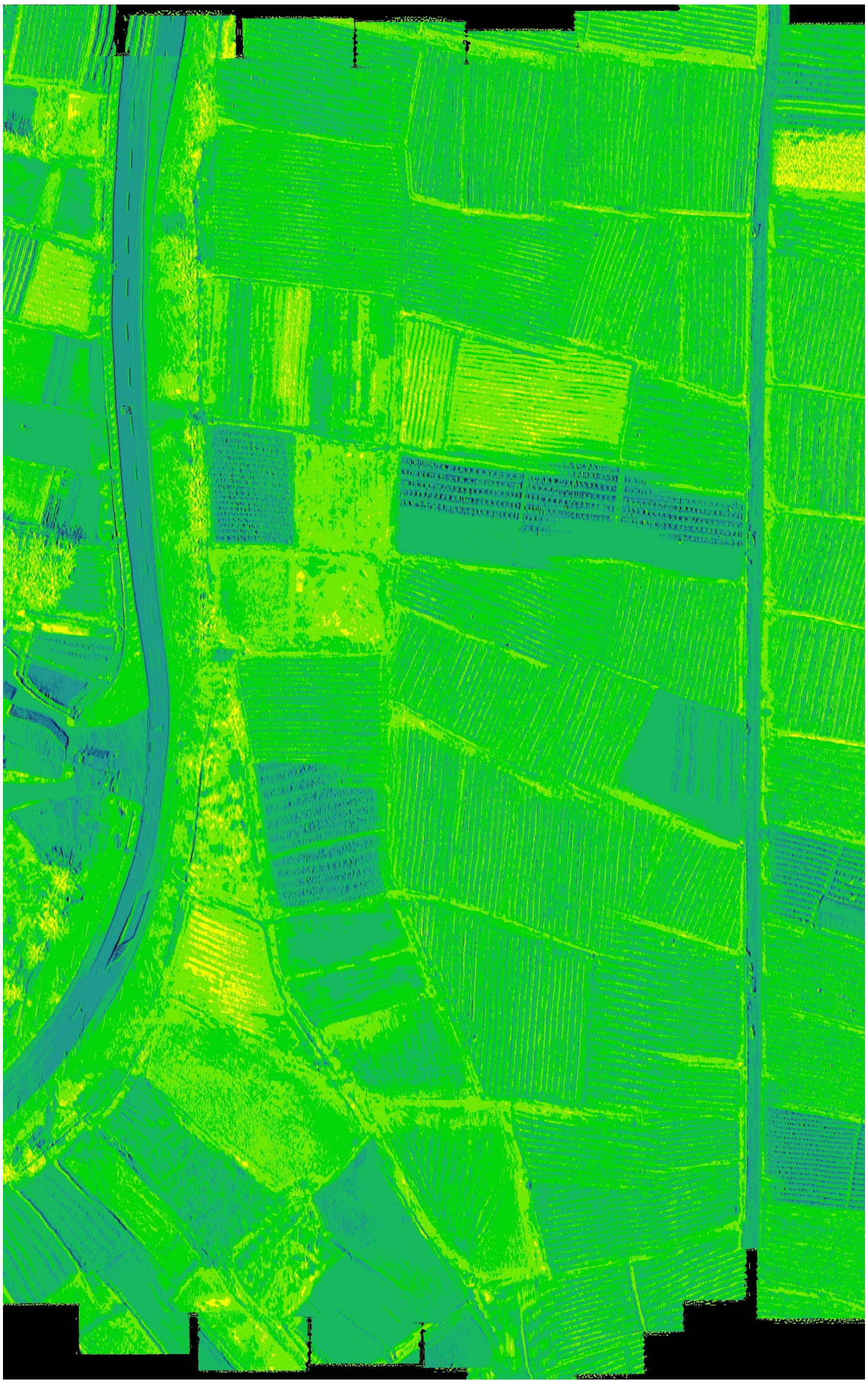

Figure 48. Crop nutrient inspection map. The darker the color, the poorer the plant health index and the lack of nutrients, and the need to take measures.

1503 Bld. A04, 3rd Software Park, Jimei, Xiamen, 361005, China
Tel: +86-592-6102588

6) Crop photosynthesis and carbon absorption

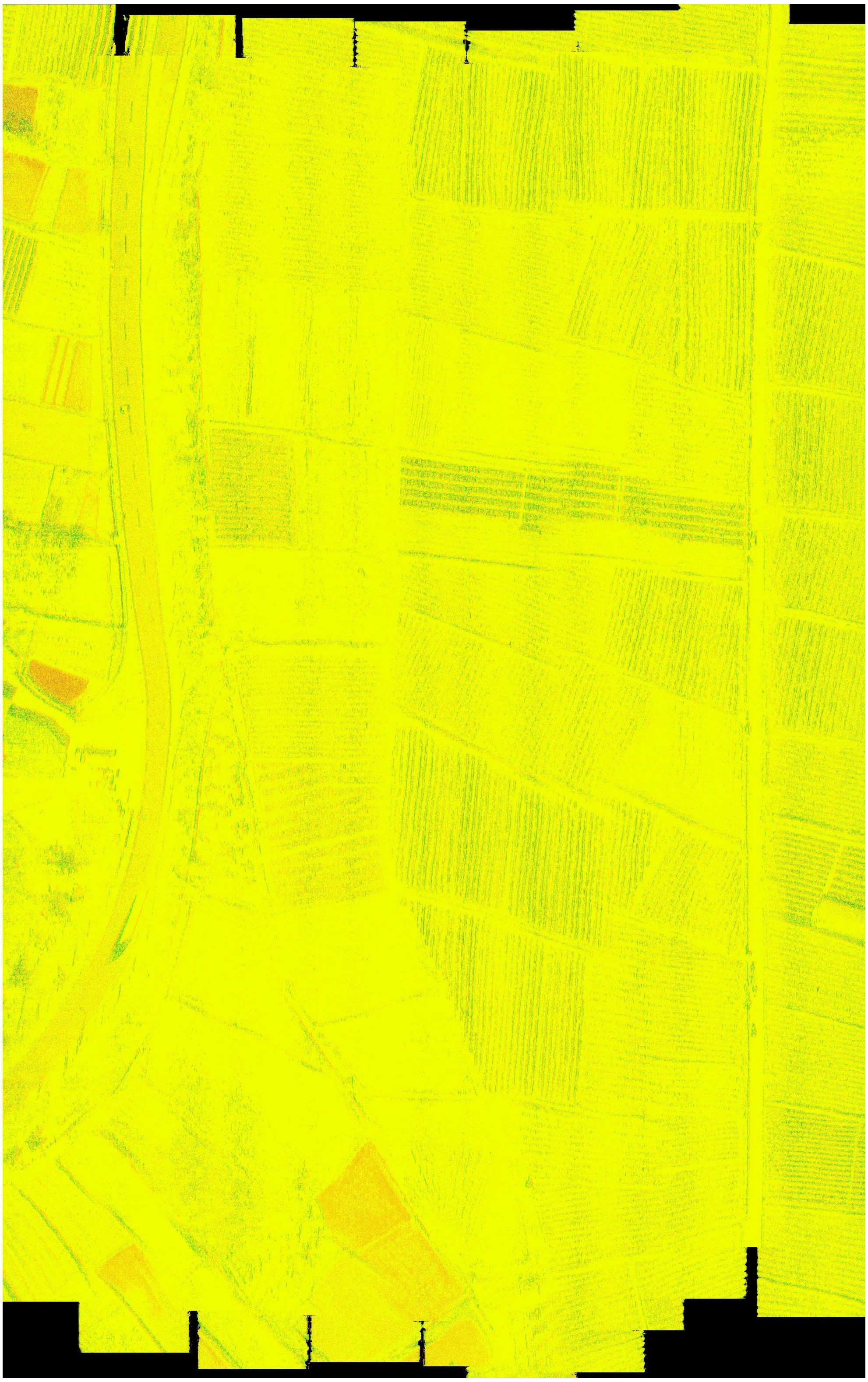

Figure 49. Crop photosynthesis and carbon absorption. The darker the color, the stronger the photosynthesis effect and the more carbon emissions absorbed.

1503 Bld. A04, 3rd Software Park, Jimei, Xiamen, 361005, China
Tel: +86-592-6102588

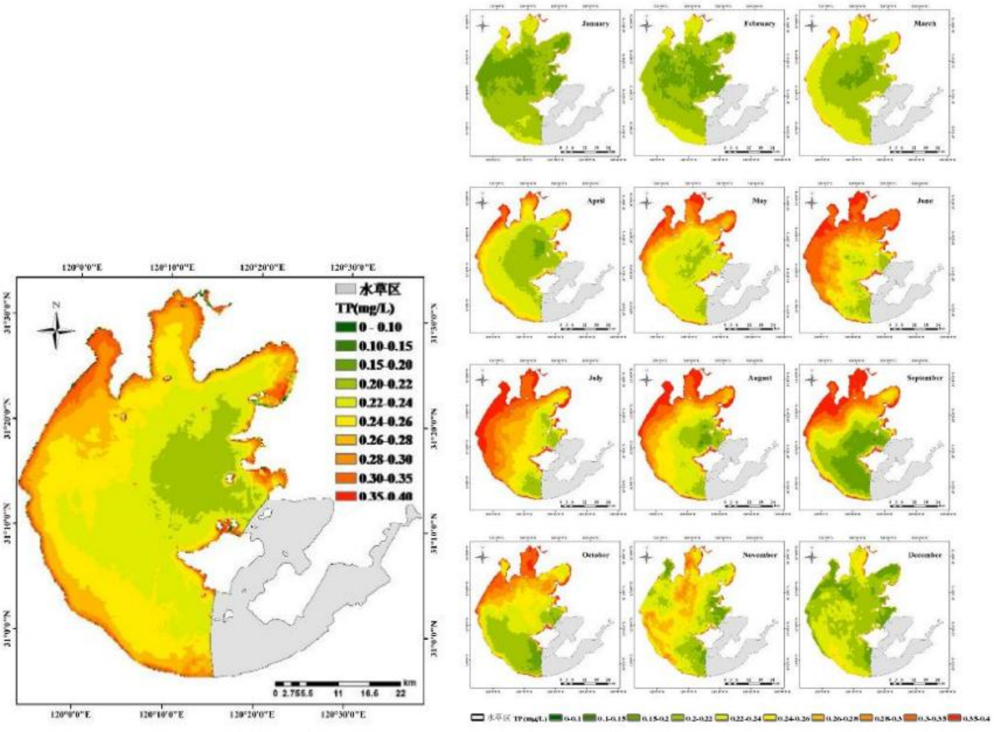

Figure 50.(a) Spatial distribution map of total phosphorus concentration in Taihu Lake. The spatial difference in total phosphorus concentration is obvious, with the highest value being 0.38mg/L and the lowest value being 0.06mg/L;

(b) The monthly variation pattern of total phosphorus concentration in different lake areas, and the lake areas are also basically the same. The maximum total phosphorus concentration was reached between June and September. The total phosphorus concentration in Zhushan Bay, Meiliang Bay and the west coast of Taihu Lake was higher than the average concentration of the entire lake from March to October of the year, and was significantly greater than that in the rest of Taihu Lake. The total phosphorus concentration in Gonghu Bay was only higher than that in June. The total phosphorus concentration in the whole lake, the total phosphorus concentration in the south bank of Taihu Lake and the greater Taihu Lake is relatively low throughout the year.

1503 Bld. A04, 3rd Software Park, Jimei, Xiamen, 361005, China
Tel: +86-592-6102588

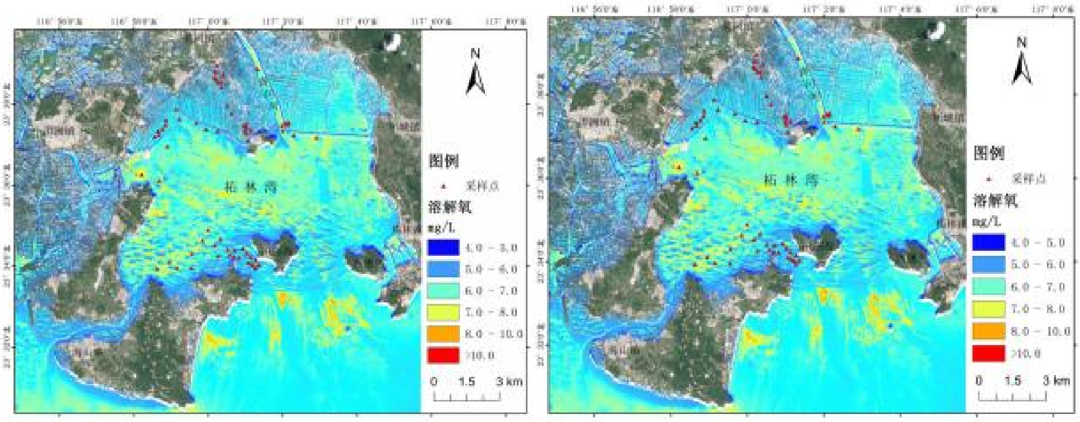

Figure 51. Dissolved oxygen and chlorophyll concentration distribution map of Zhelin Bay in eastern Guangdong taken by hyperspectral